Journal of Photochemistry & Photobiology, A: Chemistry 405 (2021) 112957

Contents lists available at ScienceDirect

Journal of Photochemistry & Photobiology, A: Chemistry

journal homepage: www.elsevier.com/locate/jphotochem

Excited-state behavior and photoinduced electron transfer of pH-sensitive Ir(III) complexes with cyclometallation (C/N–) ratios between 0/6 and 3/3

Cédric Lentz [a], Lionel Marcélis [a], Ludovic Troian-Gautier [b], Koen Robeyns [a], Emilie Cauët [c], Benjamin Elias [a,*]

[a] Université Catholique De Louvain (UCLouvain), Institut de La Matière Condensée et des Nanosciences (IMCN), Molecular Chemistry, Materials and Catalysis (MOST), Place Louis Pasteur 1, Bte L4.01.02, 1348 Louvain-la-Neuve, Belgium
[b] Laboratoire De Chimie Organique, Université libre De Bruxelles (ULB), CP 160/06, 50 Avenue F.D. Roosevelt, 1050 Brussels, Belgium
[c] Spectroscopy, Quantum Chemistry and Atmospheric Remote Sensing (CP 160/09), Université libre De Bruxelles, 50 Av. F. D. Roosevelt, B-1050 Brussels, Belgium

ARTICLE INFO

Keywords:
Iridium
Cyclometallation
Excited-state
Protonation
Photo-Induced electron transfer

ABSTRACT

The first coordination sphere of Ir(III) 2,2′-bipyridine / 2-phenylpyridine complexes can be tuned to achieve either C– or N–chelation in ratios that range between 0/6 and 3/3. Of particular interest is the synthesis of Ir(III) complexes bearing a 2,2′-bipyridine ligand coordinated in a N,C^3 pattern, leaving an exposed pyridine moiety, accessible for acid-base chemistry or coordination to a second transition metal center. The protonated forms of these "rolled-over" Ir(III) complexes were isolated in a straight-forward procedure using trifluoroacetic acid. The photophysical, photochemical and electrochemical properties of both the protonated and unprotonated Ir(III) complexes were investigated by steady-state and time-resolved spectroscopies, as well as by density functional theory calculations. The nature of the excited states was shown to depend on both the ligand coordination pattern and protonation state of the complex. In addition, the unprotonated and protonated analogues were efficiently quenched by hydroquinone and benzoquinone in acetonitrile with quenching rate constants close to the solvent diffusion limit. The results presented herein have direct implications for proton sensitive photoredox chemistry and the development of photo-acids and photo-bases.

1. Introduction

The remarkable excited-state properties of Ir(III) complexes have contributed to their widespread use in fields such as light emitting electrochemical cells (LEECs) [1–3], organic light-emitting diodes (OLEDs) [4–7], biolabeling agents, [8–10], photocatalysts for solar energy conversion [11–13] and in organic reactions [14–19]. As with other transition metal complexes, the electrochemical, photophysical and photochemical properties of Ir(III) complexes can be modified through the judicious choice of ancillary ligands [20]. In contrast to typical transition metal complexes, Ir(III) complexes can accommodate up to three cyclometalated bonds between the metal center and the coordinating ligands [21,22]. Hence, the C/N (C–chelation *vs.* N–chelation) ratio in the first coordination sphere of Ir(III) complexes can be tuned gradually from 0/6 to 3/3. This represents a unique opportunity to achieve and study a diverse set of excited-state properties with the same metal center.

Common Ir(III) complexes are derived from the prototypical *fac*-[Ir(ppy)$_3$] (hereafter abbreviated [IrN$_3$C$_3$] (**7**)) with ppyH standing for 2-phenylpyridine. This complex has a 3/3 C/N–Ir bond ratio thanks to the formation of three cyclometalated bonds. A second very common type of Ir(III) complex, with a 2/4 C/N–Ir bond ratio, is $[Ir(C,N)_2(N,N')]^+$ (hereafter abbreviated $[IrN_4C_2]^+$ (**5**)), where N,N and C,N are 2,2′-bipyridine and 2-phenylpyridine moieties, respectively [23–33]. The lowest energy excited states of these complexes are often attributed to MLCT (Metal to Ligand Charge Transfer) and MLLCT (Metal-Ligand to Ligand Charge Transfer) transitions for [IrN$_3$C$_3$] (**7**) and $[IrN_4C_2]^+$ (**5**), respectively, and these excited states have been the subject of many photophysical and electrochemical investigations [34–37]. In contrast, $[Ir(N,N'\text{-bpy})_3]^{3+}$ and $[Ir(N,N'\text{-bpy})_2(ppy)]^{2+}$ derivatives (hereafter abbreviated $[IrN_6]^{3+}$ (**6**) and $[IrN_5C_1]^{2+}$ (**3**) respectively) have been scarcely investigated, despite being expected to display interesting photo-induced properties [38–42]. This is mostly due to the harsh conditions associated with the synthesis of these complexes. An Ir(III) complex bearing three 2,2′-bipyridine ligands, one of which was chelated with a N,C^3 pattern, represents an intermediate structure

* Corresponding author.
E-mail address: benjamin.elias@uclouvain.be (B. Elias).

https://doi.org/10.1016/j.jphotochem.2020.112957
Received 22 April 2020; Received in revised form 24 September 2020; Accepted 25 September 2020
Available online 1 October 2020

between $[IrN_6]^{3+}$ (**6**) and $[IrN_5C_1]^{2+}$ (**3**) (Fig. 1) [43–47]. Interestingly, in this "rolled-over" complex, $[R\text{-}IrN_5C_1]^{2+}$ (**4**), one nitrogen atom on the bipyridine ligand is available for acid-base, ground or excited-state chemistry [48–57]. This is of great interest in research fields where an acidic medium may influence a given photoreaction, such as in photodynamic destruction of cancer cells. Moreover, the N-tethering of a second transition metal onto an iridium(III) photosensitizer has been proven a valuable approach towards the design of efficient light harvesting devices [58–60]. Yet, the addition of a metal cation often results in dramatic changes on the overall photophysics of the supramolecular compound. Easier to achieve, protonated species represent a convenient mimic of the effect resulting from the addition of an electrophilic substituent on the outer coordination sphere of the iridium complex. Herein, the synthesis of the complex, from its corresponding precursor, [Ir(N,N'-bpy)(N,C^3-bpy)Cl_2] (hereafter abbreviated $[R\text{-}IrN_3C_1Cl_2]$ (**2**)) is reported. The photophysical, photochemical and acid-base properties of the resulting Ir(III) complexes were investigated by means of steady-state photoluminescence, ^{1}H NMR spectroscopy, Density Functional Theory (DFT) calculations and rationalized by comparison to already reported Ir(III) complexes.

2. Results and discussion

2.1. Synthesis

The synthetic strategy focused on the efficient synthesis of the [Ir(N,N'-bpy)$_2Cl_2$]$^+$ precursor (hereafter abbreviated $[IrN_4Cl_2]^+$ (**1**), Fig. 1). This synthesis was optimized using a micro-wave procedure and yielded the desired $[IrN_4Cl_2]^+$ (**1**) product with a 60 % yield, as well as the cyclometalated mononuclear analogue, [Ir(N,N'-bpy)(N,C^3-bpy)Cl_2] ($[R\text{-}IrN_3C_1Cl_2]$ (**2**)) in 31 % yield (Fig. 1) which could be easily separated by column chromatography on alumina. This precursor, coordinating a "rolled-over" pyridine ring, was previously reported by Watts and coworkers, however exclusively as a dimer [41,61]. X-Ray crystallography unambiguously confirmed the structures of both $[IrN_4Cl_2]^+$ (**1**) and $[R\text{-}IrN_3C_1Cl_2]$ (**2**) precursors. (Fig. 2 and Table S**1**).

The neutral, mononuclear $[R\text{-}IrN_3C_1Cl_2]$ (**2**) complex exhibited a $P2_1/c$ packing with the iridium center in a slightly distorted octahedral geometry. One of the chelating bonds was reported as significantly longer than the others (2.136 Å *vs* 2.016 Å, 2.031 Å and 2.046 Å). X-ray refinement indicated that the longest bond corresponded to an Ir–N bond *trans* to the shortest bond, assigned to the Ir–C bond. The values reported here coincide with common *trans* Ir–C and Ir–N bonds (2.012 Å and 2.150 Å, respectively) in octahedral Ir(III) complexes. These observations also concur with crystallographic data for the $[Ir(ppy)_2Cl]_2$ dimer, where the Ir–C and Ir–N bonds were determined to be 2.052 Å and 2.111 Å respectively [2]. These observations clearly suggested that the Ir–C bond was favored in the *trans* position with respect to the second N,N'-bpy ligand, which has a stronger π-acceptor character than the chlorides.

$[IrN_4Cl_2]^+$ (**1**) is isostructural with $[R\text{-}IrN_3C_1Cl_2]$ (**2**) with a RMSD of 0.269 Å and is located on a crystallographic 2-fold axis. All Ir–N are very similar, 2.046 and 2.049 Å, respectively. A search in the CSD database [62] shows that the Ir–N bond is on average 0.038(16) Å longer than the Ir-C bond for N,C coordinated 2,2′-bipyridine and 2-phenylpyridine moieties. The same trend is observed in $[R\text{-}IrN_3C_1Cl_2]$ (**2**) where Ir–N (2.046 Å) is 0.03 Å longer than Ir-C (2.016 Å).

$[R\text{-}IrN_5C_1]^{2+}$ (**4**) was then obtained through the reaction of $[R\text{-}IrN_3C_1Cl_2]$ (**2**) with a third 2,2′-bipyridine ligand in refluxing ethylene glycol. The corresponding stable protonated forms, *i.e.* $[R\text{-}IrN_3C_1Cl_2\text{-}H]^+$ (**2-H**$^+$) and $[R\text{-}IrN_5C_1\text{-}H]^{3+}$ (**4-H**$^+$), were isolated by the addition of trifluoroacetic acid in an acetonitrile solution, followed by the addition of diethylether to precipitate the corresponding protonated Ir(III) complexes.

The synthesis of $[IrN_5C_1]^{2+}$ (**3**) was achieved by first reacting $[IrN_4Cl_2][IrN_4Cl_2]^+$ (**1**) with triflic acid in *o*-dichlorobenzene to generate the corresponding $[Ir(bpy)_2(OTf)_2](OTf)$ complex. This complex was then reacted with 2-phenylpyridine in 2-ethoxyethanol and the final product was obtained after purification on silica preparative chromatography plate. $[IrN_6]^{3+}$ (**6**) was obtained in 80 % yield by reaction of $[Ir(bpy)_2(OTf)_2](OTf)$ with 2,2′-bipyridine in ethylene glycol under argon.

$[IrN_4C_2]^+$ (**5**) was prepared following a standard route involving the synthesis of the dichloro-bridged dimer $Ir(ppy)_2(\mu\text{-}Cl)]_2$ following Nonoyama's approach [63]. This dimer was then reacted with 2,2′-bipyridine in CH_3CN/EtOH mixtures to yield $[IrN_4C_2]^+$ (**5**) in 88 % yield. $[IrN_3C_3]$ (**7**) was obtained when $[Ir(ppy)_2(\mu\text{-}Cl)]_2$ was first activated with acetonitrile to generate $[Ir(ppy)_2(CH_3CN)_2](PF_6)$ which was then allowed to react with 2-phenylpyridne in *o*-dichlorobenzene. $[IrN_3C_3]$ (**7**) was obtained in 47 % yield after purification by column chromatography on silica gel.

2.2. pKa determination by NMR spectroscopy

^{1}H NMR spectroscopy is commonly used for the characterization of polyazaaromatic Ir(III) complexes. However, despite the inherent symmetry of the N,C^3-chelated 2,2′-bipyridine ligand, comprehensive ^{1}H assignment in complexes such as $[R\text{-}IrN_5C_1]^{2+}$ (**4**) is not straightforward due to: (i) metal induced change in chemical and magnetic environment upon complexation and (ii) the inherent asymmetry of the complex due to the cyclometalated bond between one of the pyridine residues and the Ir(III) center. Clear-cut and detailed ^{1}H assignments of the $[R\text{-}IrN_5C_1]^{2+}$ (**4**) complex using long-range inter-ligand NOEs are provided in the supplementary information. All ^{1}H signals were assigned using ^{1}H–^{1}H Correlation Spectroscopy Double Quantum Filter (COSY-DQF). The three-spin system of the cyclometalated pyridine residue wasre identified along with the four-spins systems for the N-chelated pyridine moieties which are clearly labeled in Fig. 3. Selective Nuclear Overhauser Effect Spectroscopy (NOESY) and Rotating frame Overhauser Effect Spectroscopy (ROESY) experiments were necessary to clearly differentiate each ligand with respect to one another (Fig. 3) and complete the assignment of the NMR signals.

The pKa of $[R\text{-}IrN_5C_1\text{-}H]^{3+}$ (4-H$^+$) was determined by ^{1}H NMR spectroscopy through the existing relation between pH change and chemical shifts [64]. Note that as the ^{1}H NMR experiments were performed in D_2O with a pH meter calibrated in non-deuterated solvents,

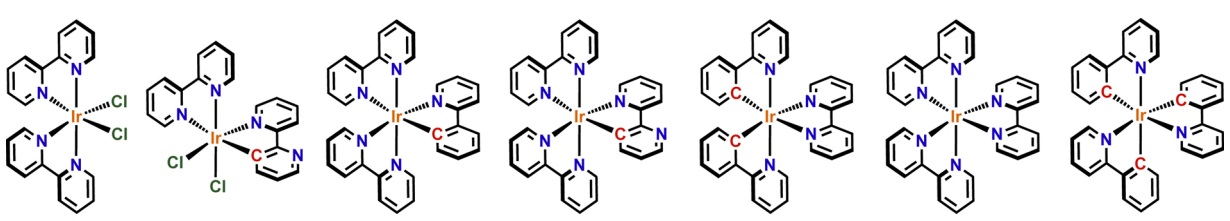

Fig. 1. Structures of the iridium(III) complexes of interest.

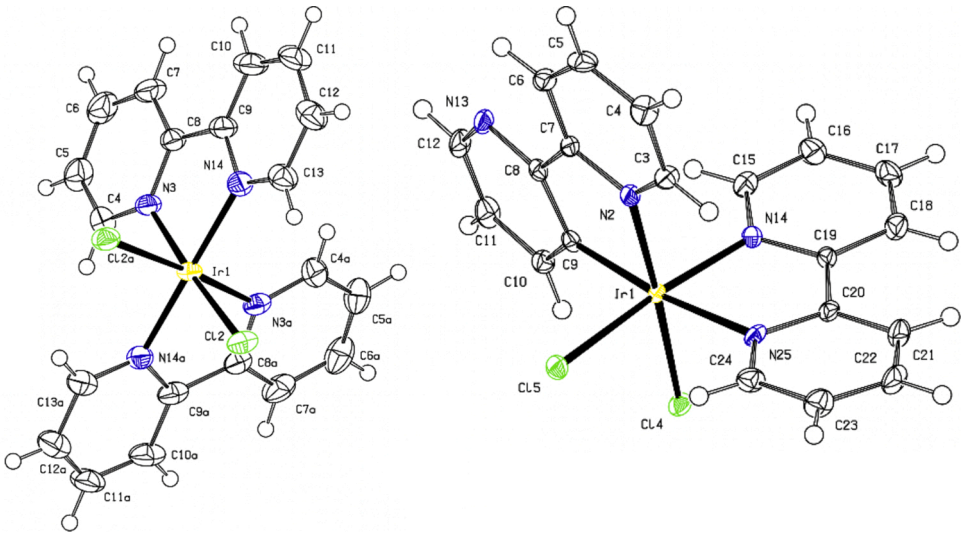

Fig. 2. ORTEP diagram of $[IrN_4Cl_2]^+$ (**1**) (left) and $[R\text{-}IrN_3C_1Cl_2]$ (**2**) (right) with the ellipsoids drawn at the 50 % probability level. A triflate anion and an acetonitrile molecule were omitted for clarity.

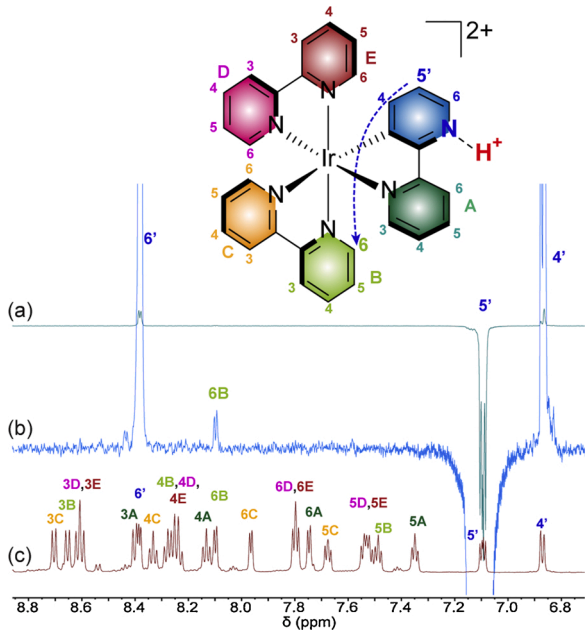

Fig. 3. Chemical structure and (a,b) ROESY-1D spectrum of $[R\text{-}IrN_5C_1]^{2+}$ (**4**) with selective excitation of N,C^3-bpy H-5′ (D_2O, 14.1 T, 25 °C, τ_m =500 ms) and (c) corresponding equilibrium ^1H spectrum with full ^1H attribution for $[R\text{-}IrN_5C_1]^{2+}$ (**4**) in D_2O.

the measurements corresponded to $pH^\dagger$ and $pKa^\dagger$, which were converted to pH and pKa respectively, according to **equations 1** and **2** [65].

$$pH = (0.929 \pm 0.001) \times pH^\dagger + (0.42 \pm 0.01) \quad (1)$$

$$pKa = (0.929 \pm 0.001) \times pKa^\dagger + (0.42 \pm 0.01) \quad (2)$$

The evolution of the ^1H NMR spectrum of $[R\text{-}IrN_5C_1]^{2+}$ (**4**) with the variation of $pH^\dagger$ is shown in Fig. 4. As expected, ^1H resonances close to the protonation site (*i.e.* H-4′ of the cyclometalated pyridine unit; see SI) shifted dramatically with pH. Fig. 4 depicts the chemical shifts of H-3B and H-4′ with changes in $pH^\dagger$ ($0 < pH^\dagger < 4$). The inflection point indicated a $pKa^\dagger$ of 1.72 and 1.82 respectively, *i.e.* pKa of 2.02 and 2.11 after correction (Eq. 2).

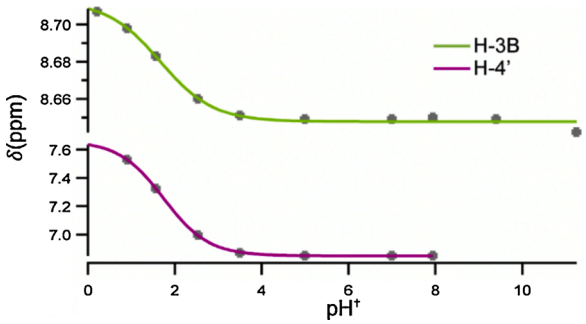

Fig. 4. Evolution of the chemical shifts for H-3B and H-4′ *vs* $pH^\dagger$. The chemical shift for H-4′ is not well defined at $pH^\dagger = 0.21$ due to the superimposition of several signals in the spectrum.

2.3. Electrochemistry

All Ir(III) complexes, including the protonated and deprotonated forms of $[R\text{-}IrN_3C_1Cl_2]$ (**2**) and $[R\text{-}IrN_5C_1]^{2+}$ (**4**) were electrochemically characterized in 0.1 M tetrabutylammonium perchlorate ($TBAClO_4$) CH_3CN electrolytes. The electrochemical potentials associated with iridium centered oxidation and ligand centered reduction events are gathered in Table 1. Increasing the number of Ir–C bonds resulted in easier iridium centered oxidation events, a direct consequence of the increased electron density afforded by the cyclometalating Ir-C bond. This increased electron density was also accompanied by ligand-centered reductions that shifted to more negative potentials (Table 1).

Table 1
Electrochemical data for the indicated iridium (III) complexes.

Complex	$E_{1/2}(Ir^{(IV/III)})$[a]	$E_{1/2}(L^{(n/n-1)})$[a]
$[IrN_4Cl_2]^+$ (**1**)	> +2.0	-1.08^r, -1.32^r
$[R\text{-}IrN_3C_1Cl_2]$ (**2**)	$+1.38^r$	-1.29^r
$[R\text{-}IrN_3C_1Cl_2\text{-}H]^+$ (**2-H$^+$**)	$+1.60^{ir}$	-1.04^{ir}, -1.36^{ir}
$[IrN_5C_1]^{2+}$ (**3**)	$+1.78^{ir}$	-1.04^r, -1.24^r
$[R\text{-}IrN_5C_1]^{2+}$ (**4**)	> +2.0	-1.07^r, -1.27^r
$[R\text{-}IrN_5C_1\text{-}H]^{3+}$ (**4-H$^+$**)	> +2.0	-0.95^r, -1.16^r
$[IrN_4C_2]^+$ (**5**)	$+1.33^r$	-1.32^r
$[IrN_6]^{3+}$ (**6**)	> +2.0	-1.03^r, -1.22^{ir}
$[IrN_3C_3]$ (**7**)	$+0.80^r$	< –2.0

[a] in V *vs.* Ag/AgCl. Experiments were performed in CH_3CN with 0.1 M $TBAClO_4$ as supporting electrolyte. r = reversible, ir = irreversible.

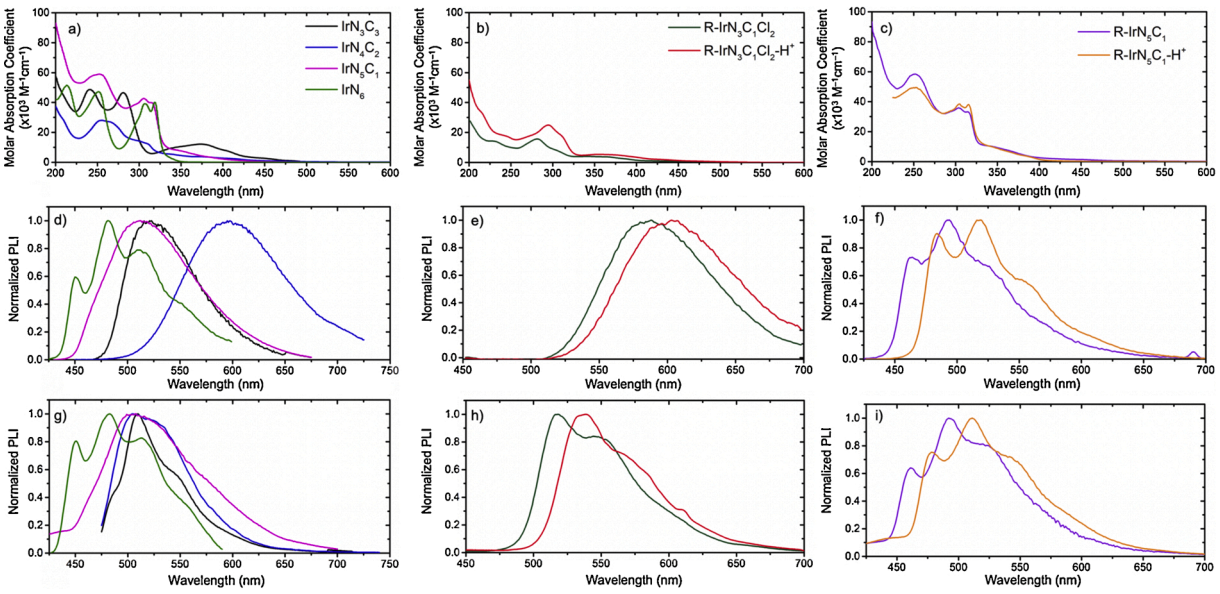

Fig. 5. Absorption (a, b, c) and photoluminescence spectra recorded at room temperature in CH_3CN (d, e, f) or in EtOH/MeOH at 77 K (g, h, i) of the indicated iridium complexes. The color code is: $[IrN_3C_3]$ (**7**) (black), $[IrN_4C_2]^+$ (**5**) (blue), $[IrN_5C_1]^{2+}$ (**3**) (magenta), $[IrN_6]^{3+}$ (**6**) (green), $[R\text{-}IrN_3C_1Cl_2]$ (**2**) (olive), $[R\text{-}IrN_3C_1Cl_2\text{-}H^+]$ (**2-H$^+$**) (red), $[R\text{-}IrN_5C_1]^{2+}$ (**4**) (purple) and $[R\text{-}IrN_5C_1\text{-}H^+]^{3+}$ (**4-H$^+$**) (orange).

The metal centered oxidation at +1.38 V *vs.* Ag/AgCl for $[R\text{-}IrN_3C_1Cl_2]^{2+}$ (**2**) was strongly affected by the presence of the cyclometalating bond, as the oxidation potential of the corresponding $[IrN_4Cl_2]^+$ (**1**) complex occurred at a potential greater than +2 V *vs.* Ag/AgCl [66]. A single reversible ligand-centered reduction wave at –1.29 V *vs.* Ag/AgCl was measured for $[R\text{-}IrN_3C_1Cl_2]$ (**2**). This reduction was reasonably assigned to the most electron accepting ligand, *i.e.* the N,N'-bpy moiety [67]. The more negative potential required to reduce the N,N'-bpy ligand in $[R\text{-}IrN_3C_1Cl_2]$ (**2**) compared to $[IrN_4Cl_2]^+$ (**1**) was a consequence of the Ir–C *trans* effect observed in the X-ray structure, which raises the energy of the π*(N,N'-bpy). This observation was also confirmed through DFT calculations (*vide infra)*.

Regarding $[R\text{-}IrN_5C_1]^{2+}$ (**4**), the one-electron oxidation occurred at a more positive potential (> 200 mV) than that of $[IrN_5C_1]^{2+}$ (**3**). This came from the decreased electron density of the cyclometalating bond due to the rolled-over bipyridine. For $[R\text{-}IrN_5C_1]^{2+}$ (**4**), two reversible ligand-centered reduction processes at –1.07 V and –1.27 V *vs.* Ag/AgCl were measured. These electrochemical processes were similar to the reduction events measured for the structurally related compound, $[IrN_5C_1]^{2+}$ (**3**).

Protonation had drastic effects on the electrochemical potentials. Indeed, protonation of $[R\text{-}IrN_5C_1]^{2+}$ (**4**) resulted in reversible ligand-centered reduction waves that were shifted to more positive potentials compared to the unprotonated complex, *i.e.* –0.95 V and –1.16 V *vs.* Ag/AgCl. This shift was consistent with the electron withdrawing effect caused by protonation of the pendant pyridine moiety. Similar observations were made for $[R\text{-}IrN_3C_1Cl_2\text{-}H]^+$ (**2-H$^+$**) where both ligand-centered reductions and the metal-centered oxidation were shifted to more positive potentials. Since both of these reductions are centered on the N,N'-bpy ligand, it was proposed that the protonation decreased the *trans* Ir–C effect on the N,N'-bpy ligand, hence causing an anodic shift of the reduction potentials. In addition, protonation also induced a stabilization of the π and π* orbitals located on the rolled-over N,C^3-bpy.

2.4. Photophysical properties

The absorption and photoluminescence spectra of all iridium (III) complexes are gathered in Fig. 5. They exhibit intense ground-state absorption features below 350 nm with more moderately intense absorption features in the visible range (between 80 and 2700 M^{-1} cm^{-1} at 450 nm for IrN_6 (**6**) and IrN_3C_3 (**7**), respectively). The molar absorption coefficients of the different complexes were in the range of values reported for similar complexes [30,43,68–70]. The simulated TD-DFT absorption spectra of all iridium (III) complexes in their ground-state singlet geometries are presented in Figs. S15-S22. The heights of the excitation lines are proportional to relevant oscillator strengths (*g*). Protonation of $[R\text{-}IrN_3C_1Cl_2]$ (**2**) induced a redshift of *ca* 10–15 nm of the ground-state absorption features, which implied that the orbitals involved in the spectroscopic processes were sensitive to protonation. On the contrary, the ground-state absorption features of the rolled-over $[R\text{-}IrN_5C_1]^{2+}$ (**4**) were almost insensitive to protonation with small spectral changes observed in the UV region and around 430 nm.

Visible light excitation of these Ir(III) complexes resulted in intense photoluminescence (Fig. 5) with quantum yields that ranged from 0.002 to 0.182 and excited-state lifetimes that ranged from 20 ns to 6.34 μs under inert atmosphere (Table 2). It is generally accepted that a manifold of excited states contributes to the overall photophysics of Ir(III) complexes [72]. Usually, a dominant character (like Ligand-Centered (LC), Metal-to-Ligand Charge Transfer (MLCT), Metal-Ligand-to-Ligand Charge Transfer (MLLCT)) is used to describe the excited-state features. For $[R\text{-}IrN_3C_1Cl_2]$ (**2**), the short excited-state lifetime and broad unresolved photoluminescence was consistent with a charge transfer (CT) type excited-state, rather than pure ligand-centered (^{3}LC) transition. In addition, k_r values (Table 2) were relatively large compared to values associated with pure ^{3}LC transitions. Hence, the excited-state of $[R\text{-}IrN_3C_1Cl_2]$ (**2**) was proposed to be a ^{3}MLLCT transition between the "Ir-C(N,C^3-bpy)" moiety and the ancillary N,N'-bpy ligand. Both $[R\text{-}IrN_3C_1Cl_2]$ (**2**) and its protonated form undergo a blueshift of the photoluminescence spectra, accompanied by the appearance of structured features when the temperature was lowered from 298 K to 77 K (Fig. 5). Protonation of the rolled-over 2,2′-bipyridine ligand induced electron deficiency on the cyclometalated N,C^3-bpy-H$^+$ ligand. This prompted a shift in the LUMO from the N,N'-bpy ligand to the N,C^3-bpy-H$^+$ ligand. This electron deficiency on the cyclometalated ligand also affected the electron density on the metal center, where the HOMO was found to be more localized on the Ir metal center after protonation. In $[R\text{-}IrN_3C_1Cl_2]$ (**2**), DFT results showed that the HOMO was localized on the Ir metal center as well as on the Ir-C(N,C^3-bpy) moiety while the LUMO was centered on the N,N'-bpy ligand (Fig. 6). The DFT calculations performed on the protonated species

Table 2
Photophysical data for the indicated complexes.

Complex	PL_{max} [a] CH_3CN (nm)	PL_{max} [a,b] H_2O (nm)	PL_{max} [a,c] 77 K (nm)	τ [d](μs)	φ [e]	k_r [f]($x10^3$ s^{-1})
$[IrN_4Cl_2]^+$ (**1**)	533	—	477, 509, 547	0.412 (0.296)	0.016	38.8
$[R\text{-}IrN_3C_1Cl_2]$ (**2**)	586	—	518, 548	0.020	0.002	102.6
$[R\text{-}IrN_3C_1Cl_2\text{-}H]^+$ (**2-H$^+$**)	602	—	537, 569	0.117	0.008	68.4
$[IrN_5C_1]^{2+}$ (**3**)	507	503	490	2.770 (0.595)	0.139	50.2
$[R\text{-}IrN_5C_1]^{2+}$ (**4**)	464, 493, 523	461, 491, 521	453, 483, 515	0.298 (0.282)	0.182	611.8
$[R\text{-}IrN_5C_1\text{-}H]^{3+}$ (**4-H$^+$**)	484, 516, 557	482, 513, 552	469, 502, 533	5.780 (1.03)	0.021	3.63
$[IrN_4C_2]^+$ (**5**)	587	600	507	0.307 (0.063)	0.035	114.0
$[IrN_6]^{3+}$ (**6**)	452, 484, 514	452, 484, 514	451, 483, 515	6.340 (1.24)	0.129	20.3
$[IrN_3C_3]$ (**7**)	517	Not sol.	486, 510, 549	0.864[g] (0.020)	0.040	46.3

[a] λ_{exc} =400 nm. [b] Measured in phosphate buffer 50 mM, H_2O milliQ, pH = 7.0. [c] Measured in EtOH/MeOH (4:1) matrix. [d] In acetonitrile under argon with values for air-equilibrated solution in parenthesis. [e] The quantum yield (± 5%) was measured under argon using $[Ru(bpy)_3]^{2+}$ as reference; φ_{ref} = 0.028 in H_2O, λ_{exc}=400 nm, and 298 K. [f] Radiative rate constant at 298 K ($k_r = \varphi/\tau$). [g] Self-quenching process due to aggregation of $[IrN_3C_3]$ (**7**) complex in CH_3CN. The luminescence lifetime of $[IrN_3C_3]$ (**7**) isolated in CH_3CN is reported as 1.74 μs under argon. [71].

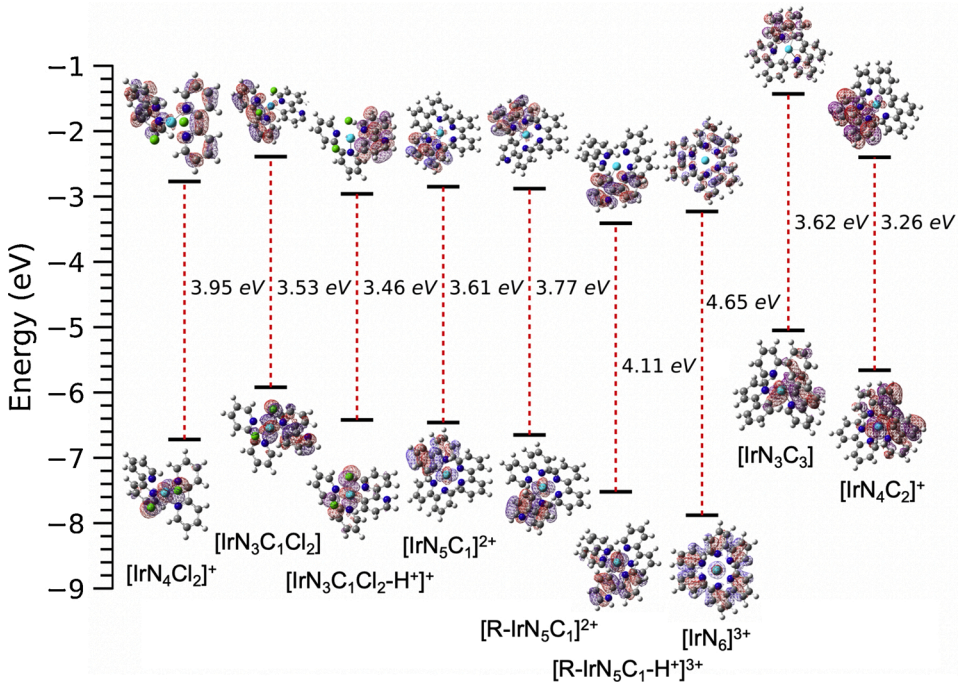

Fig. 6. Comparison of the frontier molecular orbitals of the Ir(III) complexes with their HOMO-LUMO gaps.

predicted a change in the transition, as after protonation the HOMO was mainly centered on the metal center while the LUMO was located on the N,C^3-bpy-H^+ ligand instead. The photoluminescence maxima were also determined by DFT calculations using the T_1 to S_0 energy differences. This yielded photoluminescence maxima of 500 nm for the unprotonated complex and 539 nm for the protonated complex whereas the experimentally determined value at 77 K were measured at 518 and 537 nm for the unprotonated and protonated complex, respectively. Overall, DFT calculations were were in full agreement with the above observations.

The room temperature photoluminescence spectra of $[R\text{-}IrN_5C_1]^{2+}$ (**4**) and $[R\text{-}IrN_5C_1\text{-}H^+]^{3+}$ (**4-H$^+$**) exhibited vibronic structure (Fig. 5) with the PL spectra of $[R\text{-}IrN_5C_1\text{-}H^+]^{3+}$ (**4-H$^+$**) being red-shifted by 26 nm compared to the unprotonated analogue. Furthermore, the electron-withdrawing character of the non-chelating nitrogen in $[R\text{-}IrN_5C_1]^{2+}$ (**4**) compared to $[IrN_5C_1]^{2+}$ (**3**) induced a 20 nm blue-shift of the PL spectra, consistent with a stabilization of the HOMO level. This agreed with the electrochemical data, where $[R\text{-}IrN_5C_1]^{2+}$ (**4**) was oxidized at more positive potential than $[IrN_5C_1]^{2+}$ (**3**). The excited-state lifetime of the rolled-over $[R\text{-}IrN_5C_1]^{2+}$ (**4**) was long-lived, *i.e.* 5.78 μs, which was in the same range as the one measured for $[IrN_6]^{3+}$ (**6**) *i.e.* 6.34 μs. When the solvent was switched from acetonitrile to water, only minor solvatochromic effects were observed (Table 2). In addition, the photoluminescence spectra also remained unaltered when recorded at 77 K. Altogether, these spectroscopic data, as well as the small radiative rate constant, $k_r = 20.3 \times 10^3$ s^{-1}, were more consistent with a ^{3}LC excited-state for the rolled-over $[R\text{-}IrN_5C_1]^{2+}$ (**4**) with small contributions from ^{3}MLLCT transitions. Experimental data and theoretical calculations (see Supporting Information for details) allowed to suggest an assignment for the dominant excited-state character for these iridium (III) complexes, Table 3.

2.5. Photochemistry of the tris-chelated complexes

The excited-state oxidation and reduction potentials were estimated using Eq.s 3 and 4, where $E_{1/2}(Ir^{(n/n-1)})$ and $E_{1/2}(Ir^{(n+1/n)})$ represent the potential of the first reduction and oxidation, respectively. E_{00} represents the energy stored in the excited-state, which was estimated by Franck-Condon lineshape analysis of the photoluminescence spectra (Table S2). The excited-state oxidation ($E_{1/2}(Ir^{(n+1/n)*})$) and reduction ($E_{1/2}(Ir^{(n/n-1)*})$) potentials are gathered in Table 4.

Table 3
Excited-state character of the indicated Ir(III) complexes. Assignements were made based on experimental data and theoretical DFT calculations (see SI for details).

Complex	Proposed excited-state	HOMO
$[IrN_4Cl_2]^+$ (**1**)	^{3}MLLCT	Ir-Cl
[R-$IrN_3C_1Cl_2$] (**2**)	^{3}MLLCT	Ir-C(N,C^3-bpy)
[R-$IrN_3C_1Cl_2$-H]$^+$ (**2-H$^+$**)	^{3}MLLCT	Ir-C(N,C^3-bpy-H$^+$)
$[IrN_5C_1]^{2+}$ (**3**)	^{3}MLLCT/^{3}LC	Ir-C(ppy)/π(N,N'-bpy)
[R-IrN_5C_1]$^{2+}$ (**4**)	^{3}MLLCT/^{3}LC	Ir-C(N,C^3-bpy)
[R-IrN_5C_1-H]$^{3+}$ (**4-H$^+$**)	^{3}MLLCT	π(N,N'-bpy)
$[IrN_4C_2]^+$ (**5**)	^{3}MLLCT	Ir-C(ppy)
$[IrN_6]^{3+}$ (**6**)	^{3}LC	π(N,N'-bpy)
$[IrN_3C_3]$ (**7**)	^{3}MLLCT	Ir-C(ppy)

$$E_{\frac{1}{2}}\left(Ir^{n/n-1*}\right) = E_{\frac{1}{2}}\left(Ir^{n/n-1}\right) + E_{00} \quad (3)$$

$$E_{\frac{1}{2}}\left(Ir^{n+1/n*}\right) = E_{\frac{1}{2}}\left(Ir^{n+1/n}\right) - E_{00} \quad (4)$$

These excited-state redox potentials highlighted that all complexes presented herein could be used for photo-induced electron transfer reactions with appropriate substrates. Thus, photo-triggered reactions were investigated in the presence of a model electron donor (D) *i.e.* hydroquinone (H_2Q), or electron acceptor (A) *i.e.* benzoquinone (BQ). The driving force (ΔG_{ET}) for excited-state electron transfer from hydroquinone or to benzoquinone was estimated according to **equations 5** and **6**, where $E_{1/2}(D^{+/0})$ and $E_{1/2}(A^{0/-})$ are the ground-state potentials of the donor or acceptor, and F is Faraday's constant.

$$\Delta G_{ET} = \left[E_{\frac{1}{2}}\left(D^{+/0}\right) - E_{\frac{1}{2}}\left(Ir^{n/n-1*}\right)\right]F \quad (5)$$

$$\Delta G_{ET} = \left[E_{\frac{1}{2}}\left(Ir^{n+1/n*}\right) - E_{\frac{1}{2}}\left(A^{0/-}\right)\right]F \quad (6)$$

These ΔG_{ET} values are gathered in Table 4 and highlight that the photoinduced electron transfer reactions were thermodynamically exothermic with most of the Ir(III) complexes. Only $[IrN_3C_3]$ (**7**) and $[IrN_4C_2]^+$ (**5**) exhibited endergonic ΔG_{ET} for the photo-induced electron transfer reaction with hydroquinone. Significantly, the driving force for the reaction with hydroquinone was almost identical with both [R-IrN_5C_1]$^{2+}$ (**4**) and [R-IrN_5C_1-H$^+$]$^{3+}$ (**4-H$^+$**). On the contrary, excited-state electron transfer from [R-IrN_5C_1-H$^+$]$^{3+*}$ (**4-H$^+$***) to benzoquinone was at least 100 meV more endergonic than with the unprotonated analogue.

The kinetics of direct electron transfer with benzoquinone or hydroquinone were investigated for all complexes by steady-state photoluminescence quenching experiments in acetonitrile under air (Fig. 7). As a representative example, the steady-state photoluminescence of [R-IrN_5C_1]$^{2+}$ (**4**) and [R-IrN_5C_1-H$^+$]$^{3+}$ (**4-H$^+$**) were efficiently quenched upon the increased concentration of either hydroquinone or benzoquinone (Fig. 7). Stern-Volmer analysis (Fig. 7**c,d**) was used to determine the corresponding quenching rate constants, k_q, which are gathered in Table 4. The quenching rate constants were, in all cases, close to the diffusion limit in acetonitrile ($k_{diff} = 1.9 \times 10^{10}$ $M^{-1}s^{-1}$) [74]. The quenching for [R-IrN_5C_1-H]$^{3+*}$ (**4-H$^+$***) in both cases were 2–3 times smaller in magnitude than for the unprotonated analogue. Hence, these excited-state quenching experiments highlighted that [R-IrN_5C_1]$^{2+}$ (**4**) and its protonated form could be used as both efficient photooxidizing or photoreducing complexes with hydro- or benzoquinone respectively.

3. Conclusions

An in-depth comparison of electrochemical, photophysical and photoredox properties of a series of Ir(III) complexes with varying number of cyclometalated bonds was achieved. An improved synthetic procedure which allowed to obtain key precursors, *i.e.* [R-$IrN_3C_1Cl_2$] (**2**) and $[IrN_4Cl_2]^+$ (**1**) and the "rolled-over" [R-IrN_5C_1]$^{2+}$ (**4**) was reported. The uncoordinated nitrogen atom in these "rolled-over" complexes was easily protonated, which led to changes in their photophysical and electrochemical properties. Electrochemical and photophysical comparative studies highlighted the key differences between these acid-base sensitive iridium(III) complexes and were compared to previously reported Ir(III) complexes. Finally, the ability of these iridium complexes to undergo photo-induced electron transfer was evidenced through steady-state photoluminescence quenching experiments that yielded quenching rate constants close to the solvent diffusion limit. Excited-state reactivity was possible with electron donors, such as hydroquinone, as well as with electron acceptors, such as benzoquinone. This highlighted the immense versatility and tunability offered by this class of Ir(III) photosensitizers for future applications in photoredox catalysis and energy conversion.

4. Materials and methods

4.1. Materials

All solvents and reagents for the synthesis were at least of reagent grade quality and were used without further purification. All solvents for the spectroscopic and electrochemical measurements were of spectroscopic grade.

4.2. Microwave synthesis

Microwave syntheses were performed on a Milestone MicroSYNTH labstation under magnetic stirring. Typical conditions allowed to reach the desired temperature in 5 min and the vessels were held at the desired temperature for the indicated period of time.

4.3. Nuclear magnetic resonance

^{1}H NMR (500 MHz) spectra were obtained on a Bruker Avance-500 instrument. Solvent residual peaks were used as internal standards for ^{1}H chemical shift referencing. NMR spectra were processed using MNOVA.

Table 4
Photophysical data for the indicated complexes in CH_3CN under argon at RT.

Complex	E_{00} (cm^{-1})	$E_{1/2}(Ir^{n+1/n})^*$ [a]	$E_{1/2}(Ir^{n/n-1})^*$ [a]	ΔG_{ET} H_2Q (eV) [b]	ΔG_{ET} BQ (eV) [b]	k_q H_2Q[c]	k_q BQ[c]
$[IrN_5C_1]^{2+}$ (**3**)	21,221	–0.85	+1.59	–0.35	–0.42	0.80	0.98
[R-IrN_5C_1]$^{2+}$(**4**)	21,565	> -0.67	+1.60	–0.36	>–0.24	3.06	3.51
[R-IrN_5C_1-H]$^{3+}$ (**4-H$^+$**)	20,707	> -0.57	+1.62	–0.38	> –0.14	1.55	1.00
$[IrN_4C_2]^+$ (**5**)	17,552	–0.85	+0.86	+0.38	–0.42	—	0.12[d]
$[IrN_6]^{3+}$(**6**)	22,163	> –0.73	+1.72	–0.48	>–0.32	0.58	1.15
$[IrN_3C_3]$ (**7**)	20,259	–1.71	< +0.51	> +0.73	–1.28	—	2.68

[a] (V *vs* Ag/AgCl). [b] Evaluated using **equations 5** and **6**, with $E_{1/2} = 1.24$ V *vs.* Ag/AgCl in CH_3CN for H_2Q, and $E_{1/2} = -0.43$ V *vs.* Ag/AgCl in CH_3CN for BQ [73]. [c] $x10^{10}M^{-1}s^{-1}$. [d] a static contribution to the quenching in presence of BQ was detected, with an estimated association constant, $K = 270$ M^{-1}.

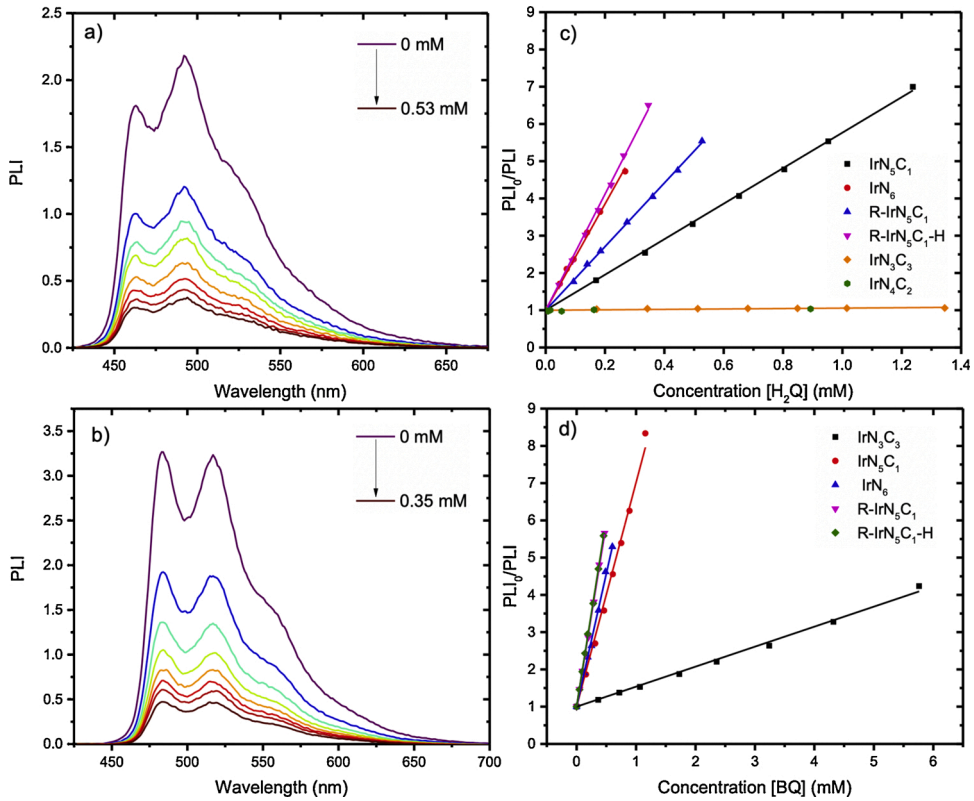

Fig. 7. Steady-state photoluminescence spectra of [R-IrN$_5$C$_1$] (**4**) (a) and [R-IrN$_5$C$_1$-H$^+$] (**4-H$^+$**) (b) with increasing amount of hydroquinone. Stern-Volmer plots, including all complexes, with hydroquinone (c) or benzoquinone (d). Experiments were performed in acetonitrile, under air and at room temperature.

4.4. Mass spectrometry

High-resolution mass spectrometry (HRMS) was recorded on a Q-Extractive orbitrap from ThermoFisher. Samples were ionized by electrospray ionization (ESI; capillary temperature =250 °C, vaporizer temperature =250 °C, sheath gas flow rate =20 mL/min).

4.5. UV – Visible absorption

UV – vis absorption spectra were recorded on a Shimadzu UV-1700 with 1 cm path length quartz cell. The molar absorption coefficients were determined by weight and absorption measurements.

4.6. Steady-state photoluminescence

Photoluminescence spectra were recorded with a Shimadzu RF-5001 PC spectrometer equipped with a Hamamatsu R-928 photomultiplier tube and with a 250 W Xenon lamp as excitation source. Measurements were performed with Ir solutions of 1×10^{-5} M. The spectra were corrected for the instrument response. The samples were excited at the maximum of the lowest absorption band for each complex. Photoluminescence intensity at 77 K was recorded on a FluoroLog3 FL3−22 from Jobin Yvon equipped with an 18 V 450 W Xenon Short Arc lamp and an R928 P photomultiplier, using an Oxford Instrument Optistat DN nitrogen cryostat controlled by an Oxford Intelligent Temperature Controller (ITC503S) instrument.

4.7. Time-resolved photoluminescence

Luminescence lifetimes measurements were performed after irradiation at λ =400 nm obtained by the second harmonic of a Titanium: Sapphire laser (picosecond Tsunami laser spectra physics 3950-M1BB+39868−03 pulse picker doubler) at a 80 kHz repetition rate. Fluotime 200 from AMS technologies was used for the decay acquisition. It consists of a GaAs microchannel plate photomultiplier tube (Hamamatsu model R3809U-50) followed by a time-correlated single photon counting system from Picoquant (PicoHarp300). The ultimate time resolution of the system is close to 30 ps. Luminescence decays were analyzed with FLUOFIT software available from Picoquant.

4.8. Electrochemistry

Cyclic voltammetry was performed in a one-compartment cell, using a glassy carbon disk working electrode (approximate area = 0.03 cm^2), a platinum counter-electrode and a saturated silver chloride reference electrode (Perkin Elmer Instruments). The potential applied to the working electrode was controlled by an Autolab Potentiostat 100 (Eco Chemie). Scan rates from 100 to 200 mV s^{-1} were used. The cyclic voltammograms were recorded in acetonitrile solutions (Acros, Acetonitrile for HPLC). The concentration of the complexes was 0.5 mM, with 0.1 M tetrabutylammonium perchlorate as supporting electrolyte. Prior to each measurement, the samples were purged with argon for 20 min.

4.9. Single crystal X-Ray diffraction

Reflection data on both crystals were collected on a MAR345 image plate detector using MoKα radiation (Rigaku Ultra X18S, rotating anode; Zr filter or Fox 3D mirror). Prior to the diffraction experiment, the crystals were flash-cooled to 150 K ([IrN$_4$Cl$_2$]$^+$ (**1**)) and 120 K ([R-IrN$_3$C$_1$Cl$_2$] (**2**)). All data were integrated using CrysAlis^{PRO} and the implemented absorption correction was applied [75]. Structures were solved by SHELXS97 and refined by full-matrix least squares on $|F^2|$ SHELXL2014/7 [76]. Non-hydrogen atoms were anisotropically refined and the hydrogen atoms were placed on calculated positions with temperature factors fixed at 1.2 times Ueq of the parent atoms and 1.5 times Ueq for methyl groups. The triflate anion in [IrN$_4$Cl$_2$]$^+$ (**1**) was found to

be located on an inversion center and was modeled in 2 superposing parts. Two void cavities were treated by the SQUEEZE procedure in Platon [77] in which no discrete solvent molecules could be located (138Å^3, 26e$^-$).

Crystallographic and refinement details are tabulated in supporting information Table S1. CCDC 155,9992−1559,993 contain the supplementary crystallographic data for this paper. The data can be obtained free of charge from The Cambridge Crystallographic Data Centre *via* www.ccdc.cam.ac.uk/structures.

4.10. Density functional theory calculations

The DFT formalism was used for all the systems. All calculations were performed using the Gaussian 09 computational chemistry package while applying default procedures, integration grids, algorithms and parameters. [78] The equilibrium geometries of the singlet and triplet states of the Ir(III) complexes were optimized in acetonitrile using the integral equation formalism model (IEFPCM) [79]. These calculations were performed using the B3LYP functional [80–82]. The 6−31 G(d,p) basis set [83–85] was used for the C, N and H atoms while the SBKJC-VDZ [86] relativistic effective core potential and associated basis set was employed to describe the Ir atoms. The harmonic vibrational frequencies of each complex have been calculated with the same level of calculation, and it has been checked that all structures correspond to true minima of the potential energy surface.

The first 25 lowest-lying excited states of the Ir complexes at their ground state singlet geometries have also been evaluated within the vertical Time-Dependent Density Functional Theory (TD-DFT) approximation. These calculations have been performed using the level of theory B3LYP/6−31 G(d,p)/ SBKJC-VDZ while the modeling of solvent effects (here acetonitrile) has been included through the IEF-PCM model.

4.11. Synthetic procedures

All the reaction mixtures were protected from direct light during the synthesis and the reactions were conducted under argon. After synthesis and purification, the compounds were characterized by ^{1}H NMR spectroscopy (500 MHz) and by high-resolution mass spectrometry unless otherwise indicated.

4.12. Bis (2,2′-bipyridine-N,N') dichloroiridium(III) hexafluorophosphate $[IrN_4Cl_2]^+$ (1) and (2,2′-bipyridine-N,N')(2,2′-bipyridine-N,C^3) dichloroiridium(III) [R-$IrN_3C_1Cl_2$] (2)

Ammonium hexachloroiridate (III) hydrate (61.3 mg, 0.128 mmol) and 2,2′-bipyridine (41.1 mg, 0.263 mmol) were suspended in ethylene glycol (5.5 mL). After being purged with argon, the suspended mixture was stirred and heated to 180 °C in a microwave (500 W) for 15 min. The solution was cooled to room temperature and a saturated aqueous solution of potassium hexafluorophosphate was added to induce precipitation. The orange solid was washed with water. The crude product was purified by column chromatography on alumina using acetone as eluent. The first collected fraction corresponded to [R-$IrN_3C_1Cl_2$] (31 %) while the second fraction corresponded to $[IrN_4Cl_2]^+$ (59 %)

Data for **[IrN4Cl2]$^+$ (1)**: HRMS (ESI): *m/z* calculated for $[C_{20}H_{16}Cl_2^{193}IrN_4 - PF_6]^+$, 575.03758 ; found: 575.03619, *m/z* calculated for $[C_{20}H_{15}Cl^{193}IrN_4 - PF_6 - HCl]^+$, 539.06090; found: 539.05982, *m/z* calculated for $[C_{20}H_{14}^{193}IrN_4 - PF_6 - 2HCl]^+$, 503.08422 ; found: 503.08599. ^{1}H NMR (CD_3CN), δ/ppm: 9.78 (dd, 2H, *H-1*, $J_{1-2} = 5.7$ Hz, $J_{1-3} = 1.5$ Hz), 8.55 (dd, 2H, *H-4*, $J_{4-3} = 8.2$ Hz, $J_{4-2} = 1.4$ Hz), 8.44 (dd, 2H, *H-5*, $J_{5-6} = 8.2$ Hz, $J_{5-7} = 1.4$ Hz), 8.37 (ddd, 2H, *H-3*, $J_{3-4} = 8.2$ Hz, $J_{3-2} = 7.8$ Hz, $J_{3-1} = 1.5$ Hz), 8.06 (ddd, 2H, *H-6*, $J_{6-5} = 8.2$ Hz, $J_{6-7} = 7.7$ Hz, $J_{6-8} = 1.4$ Hz), 7.98 (ddd, 2H, *H-2*, $J_{2-3} = 7.8$ Hz, $J_{2-1} = 5.7$ Hz, $J_{2-4} = 1.4$ Hz), 7.70 (dd, 2H, *H-8*, $J_{8-7} = 5.8$ Hz, $J_{8-6} = 1.4$ Hz), 7.38 (ddd, 2H, *H-7*, $J_{7-6} = 7.7$ Hz, $J_{7-8} = 5.8$ Hz, $J_{7-5} = 1.4$ Hz).

Data for **[R-$IrN_3C_1Cl_2$] (2)**: HRMS (ESI): *m/z* calculated for $[C_{20}H_{16}^{193}IrN_4Cl_2 + H]^+$, 575.03758; found: 575.03652, *m/z* calculated for $[C_{20}H_{15}^{193}IrN_4Cl - Cl]^+$, 539.0609; found: 539.0583. ^{1}H NMR (CD_3CN), δ/ppm: 9.79 (dd, 1H, *H-1*, $J_{1-2} = 5.4$ Hz, $J_{1-3} = 1.6$ Hz), 8.59 (dd, 1H, *H-15*, $J_{15-14} = 7.6$ Hz, $J_{15-13} = 1.7$ Hz), 8.50 (dd, 1H, *H-4*, $J_{4-3} = 7.9$ Hz, $J_{4-2} = 1.1$ Hz), 8.38 (dd, 1H, *H-13*, $J_{13-14} = 4.6$ Hz, $J_{13-15} = 1.7$ Hz), 8.32 (dd, 1H, *H-5*, $J_{5-6} = 8.2$ Hz, $J_{5-7} = 1.4$ Hz), 8.28 (ddd, 1H, *H-3*, $J_{3-4} = 7.9$ Hz, $J_{3-2} = 7.7$ Hz, $J_{3-1} = 1.6$ Hz), 8.23 (dd, 1H, *H-12*, $J_{12-11} = 8.0$ Hz, $J_{12-10} = 1.6$ Hz), 7.98 (ddd, 1H, *H-2*, $J_{2-3} = 7.7$ Hz, $J_{2-1} = 5.4$ Hz, $J_{2-4} = 1.1$ Hz), 7.91 (dd, 1H, *H-8*, $J_{8-7} = 5.8$ Hz, $J_{8-6} = 1.5$ Hz), 7.81 (ddd, 1H, *H-6*, $J_{6-5} = 8.2$ Hz, $J_{6-7} = 7.6$ Hz, $J_{6-8} = 1.5$ Hz), 7.70 (ddd, 1H, *H-11*, $J_{11-12} = 8.0$ Hz, $J_{11-10} = 7.5$ Hz, $J_{11-9} = 1.4$ Hz), 7.58 (dd, 1H, *H-9*, $J_{9-10} = 5.9$ Hz, $J_{9-11} = 1.4$ Hz), 7.26 (dd, 1H, *H-14*, $J_{14-15} = 7.6$ Hz, $J_{14-13} = 4.6$ Hz), 7.16 (ddd, 1H, *H-7*, $J_{7-6} = 7.6$ Hz, $J_{7-8} = 5.8$ Hz, $J_{7-5} = 1.4$ Hz), 6.99 (ddd, 1H, *H-10*, $J_{10-11} = 7.5$ Hz, $J_{10-9} = 5.9$ Hz, $J_{10-12} = 1.6$ Hz).

4.13. Bis (2,2′-bipyridine-N,N') bis triflate iridium(III) triflate

$[Ir(bpy)_2Cl_2]PF_6$ (18.8 mg, 0.0260 mmol) was suspended in *o*-dichlorobenzene (1.7 mL) and triflic acid (100 µL, 1.13 mmol) was added. The mixture was stirred and refluxed under argon for 1 h. After this period, the solution was cooled to room temperature and another portion of triflic acid (100 µL, 1.13 mmol) was added. The mixture was brought again to reflux for 2 h. After reaction, the mixture was cooled to room temperature and diethylether was added to induce precipitation. The solid was isolated by centrifugation and washed with diethylether (105.0 mg, 94 %). HRMS (ESI): *m/z* calculated for $[C_{22}H_{16}F_6IrN_4O_6S_2 - OTf]^+$, 803.00392; found: 803.00332. ^{1}H NMR (CD_3CN), δ/ppm: 9.21 (dd, 2H, *H-1*, $J_{1-2} = 5.7$ Hz, $J_{1-3} = 1.4$ Hz), 8.65 (dd, 2H, *H-4*, $J_{4-3} = 8.2$ Hz, $J_{4-2} = 1.4$ Hz), 8.53 (ddd, 2H, *H-3*, $J_{3-4} = 8.2$ Hz, $J_{3-2} = 7.9$ Hz, $J_{3-1} = 1.4$ Hz), 8.47 (dd, 2H, *H-5*, $J_{5-6} = 8.1$ Hz, $J_{5-7} = 1.5$ Hz), 8.17 (ddd, 2H, *H-2*, $J_{2-3} = 7.9$ Hz, $J_{2-1} = 5.7$ Hz, $J_{2-4} = 1.4$ Hz), 8.11 (ddd, 2H, *H-6*, $J_{6-5} = 8.1$ Hz, $J_{6-7} = 7.8$ Hz, $J_{6-8} = 1.4$ Hz), 7.52 (dd, 2H, *H-8*, $J_{8-7} = 6.0$ Hz, $J_{8-6} = 1.4$ Hz), 7.43 (ddd, 2H, *H-7*, $J_{7-6} = 7.8$ Hz, $J_{7-8} = 6.0$ Hz, $J_{7-5} = 1.5$ Hz). ^{19}F NMR (CD_3CN), δ/ppm: -379.83 (s, 3 F, free triflate), -380.18 (s, 6 F, chelated triflate).

4.14. Bis (2,2′-bipyridine-N,N') (2-phenylpyridine-N,C^3) iridium(III) hexafluorophosphate $[IrN_5C_1]^{2+}$ (3)

$[Ir(bpy)_2(OTf)_2]OTf$ (29.7 mg, 0.0312 mmol) was mixed in a minimum amount of 2-ethoxyethanol (0.9 mL) and heated to reflux. At this step, 2-phenylpyridine (44.6 µL, 0.312 mmol) was added. The mixture was refluxed for 1 h under argon. The solution was cooled to room temperature and a saturated aqueous solution of KPF_6 was added. After 2 days in the fridge, the solid was collected by centrifugation and purified by preparative plate on silica with CH_3CN:H_2O:$NH_4Cl_{(aq)}$ / 4:5:1 as eluent. The fraction with Rf = 0.3 was collected to afford a yellow solid (6.7 mg, 20 %). HRMS (ESI): *m/z* calculated for $[C_{31}H_{24}F_6^{193}IrN_5P - PF_6]^+$, 804.1297; found: 804.1287, *m/z* calculated for $[C_{31}H_{24}IrN_5 - 2PF_6]^{2+}$, 329.5825; found: 329.5826. ^{1}H NMR (CD_3CN), δ/ppm: 8.62 (dd, 1H, *H-3.Pyr1*, $J_{3.Pyr1-4.Pyr1} = 8.0$ Hz, $J_{3.Pyr1-5.Pyr1} = 0.6$ Hz), 8.57 (dd, 1H, *H-3.Pyr2*, $J_{3.Pyr2-4.Pyr2} = 8.1$ Hz, $J_{3.Pyr2-5.Pyr2} = 0.7$ Hz), 8.53 (dd, 1H, *H-3.Pyr3*, $J_{3.Pyr3-4.Pyr3} = 7.8$ Hz, $J_{3.Pyr3-5.Pyr3} = 0.6$ Hz), 8.51 (dd, 1H, *H-3.Pyr4*, $J_{3.Pyr4-4.Pyr4} = 7.8$ Hz, $J_{3.Pyr4-5.Pyr4} = 0.7$ Hz), 8.30 (ddd, 1H, *H-4.Pyr1*, $J_{4.Pyr1-3.Pyr1} = 8.0$ Hz, $J_{4.Pyr1-5.Pyr1} = 7.8$ Hz, $J_{4.Pyr1-6.Pyr1} = 1.5$ Hz), 8.25 (ddd, 1H, *H-4.Pyr3*, $J_{4.Pyr3-5.Pyr3} = 8.0$ Hz, $J_{4.Pyr3-3.Pyr3} = 7.9$ Hz, $J_{4.Pyr3-6.Pyr3} = 1.4$ Hz), 8.22 (ddd, 1H, *H-4.Pyr4*, $J_{4.Pyr4-3.Pyr4} = J_{4.Pyr4-5.Pyr4} = 7.8$ Hz, $J_{4.Pyr4-6.Pyr4} = 1.4$ Hz), 8.21 (dd, 1H, *H-3.Pyr5*, $J_{3.Pyr5-4.Pyr5} = 7.8$ Hz, $J_{3.Pyr5-5.Pyr5} = 0.7$ Hz), 8.20 (ddd, 1H, *H-4.Pyr2*, $J_{4.Pyr2-3.Pyr2} = 8.1$ Hz, $J_{4.Pyr2-5.Pyr2} = 7.9$ Hz, $J_{4.Pyr2-6.Pyr2} = 1.2$ Hz), 8.00 (ddd, 1H, *H-4.Pyr5*, $J_{4.Pyr5-3.Pyr5} = 7.8$ Hz, $J_{4.Pyr5-5.Pyr5} = 7.5$ Hz, $J_{4.Pyr5-6.Pyr5} = 1.5$ Hz), 7.97 (dd, 1H, *H-6.Pyr2*, $J_{6.Pyr2-5.Pyr2} = 6.0$ Hz, $J_{6.Pyr2-4.Pyr2} = 1.2$ Hz), 7.94 (dd, 1H, *H-4*, $J_{4-3} = 7.8$ Hz, $J_{4-2} = 1.1$ Hz), 7.90 (dd, 1H, *H-6.Pyr1*, $J_{6.Pyr1-5.Pyr1} = 5.5$ Hz, $J_{6.Pyr1-4.}$

$_{Pyr1}$ = 1.5 Hz), 7.70 (m, 2H, *H-6.Pyr3 + H-6.Pyr4*), 7.66 (ddd, 1H, *H-5.Pyr1*, $J_{5.Pyr1-4.Pyr1}$ = 7.8 Hz, $J_{5.Pyr1-6.Pyr1}$ = 5.5 Hz, $J_{5.Pyr1-3.Pyr1}$ = 0.6 Hz), 7.59 (dd, 1H, *H-6.Pyr5*, $J_{6.Pyr5-5.Pyr5}$ = 6.0 Hz, $J_{6.Pyr5-4.Pyr5}$ = 1.5 Hz), 7.53 (ddd, 1H, *H-5.Pyr3*, $J_{5.Pyr3-4.Pyr3}$ = 8.0 Hz, $J_{5.Pyr3-6.Pyr3}$ = 5.9 Hz, $J_{5.Pyr3-3.Pyr3}$ = 0.6 Hz), 7.51 (ddd, 1H, *H-5.Pyr4*, $J_{5.Pyr4-4.Pyr4}$ = 7.8 Hz, $J_{5.Pyr4-6.Pyr4}$ = 5.9 Hz, $J_{5.Pyr4-3.Pyr4}$ = 0.7 Hz), 7.50 (ddd, 1H, *H-5.Pyr2*, $J_{5.Pyr2-4.Pyr2}$ = 7.9 Hz, $J_{5.Pyr2-6.Pyr2}$ = 6.0 Hz, $J_{5.Pyr2-3.Pyr2}$ = 0.7 Hz), 7.23 (ddd, 1H, *H-3*, J_{3-4} = 7.8 Hz, J_{3-2} = 7.6 Hz, J_{3-1} = 0.8 Hz), 7.19 (ddd, 1H, *H-5.Pyr5*, $J_{5.Pyr5-4.Pyr5}$ = 7.5 Hz, $J_{5.Pyr5-6.Pyr5}$ = 6.0 Hz, $J_{5.Pyr5-3.Pyr5}$ = 0.7 Hz), 7.06 (ddd, 1H, *H-2*, J_{2-3} = J_{2-1} = 7.6 Hz, J_{2-4} = 1.1 Hz), 6.20 (dd, 1H, *H-1*, J_{1-2} = 7.6 Hz, J_{1-3} = 0.9 Hz).

Pyr1, Pyr2, Pyr3, Pyr4 and Pyr5 are undefined Pyridine residues

4.15. Bis (2,2′-bipyridine-N,N') (2,2′-bipyridine-N,C^3) iridium(III) hexafluorophosphate [R-IrN$_5$C$_1$]$^{2+}$ (4)

[Ir(N,N'-bpy)(N,C^3-bpy)Cl$_2$] (16.0 mg, 0.0279 mmol) and 2,2′-bipyridine (13.3 mg, 0.0852 mmol) were suspended in ethylene glycol (2.1 mL). After being purged with argon, the suspended mixture was stirred and heated to reflux overnight. The solution was cooled to room temperature and a saturated aqueous solution of potassium hexafluorophosphate was added to induce precipitation. The orange solid was washed successively with water, ethanol and diethylether to afford the desired product (4.0 mg, 15.1 %). HRMS (ESI): *m/z* calculated for $[C_{30}H_{23}F_6^{193}IrN_6P - PF_6]^+$, 805.12498; found: 805.12504, *m/z* calculated for $[C_{30}H_{23}IrN_6 - 2PF_6]^{2+}$, 330.08067; found: 330.07991. ^{1}H NMR (CD_3CN), δ/ppm: 8.63 (dd, 1H, *H-12*, J_{12-11} = 8.1 Hz, J_{12-10} = 1.1 Hz), 8.58 (dd, 1H, *H-13*, J_{13-14} = 8.1 Hz, J_{13-15} = 1.4 Hz), 8.54 (dd, 1H, *H-5*, J_{5-6} = 8.1 Hz, J_{5-7} = 1.2 Hz), 8.52 (dd, 1H, *H-4*, J_{4-3} = 8.1 Hz, J_{4-2} = 1.3 Hz), 8.47 (dd, 1H, *H-20*, J_{20-19} = 8.0 Hz, J_{20-18} = 1.6 Hz), 8.42 (dd, 1H, *H-21*, J_{21-22} = 4.7 Hz, J_{21-23} = 1.6 Hz), 8.32 (ddd, 1H, *H-11*, J_{11-12} = 8.1 Hz, J_{11-10} = 7.9 Hz, J_{11-9} = 1.6 Hz), 8.26 (ddd, 1H, *H-6*, J_{6-5} = 8.1 Hz, J_{6-7} = 8.0 Hz, J_{6-8} = 1.5 Hz), 8.24 (ddd, 1H, *H-3*, J_{3-4} = 8.1 Hz, J_{3-2} = 8.0 Hz, J_{3-1} = 1.5 Hz), 8.22 (ddd, 1H, *H-14*, J_{14-13} = 8.1 Hz, J_{14-15} = 7.7 Hz, J_{14-16} = 1.5 Hz), 8.09 (ddd, 1H, *H-19*, J_{19-20} = 8.0 Hz, J_{19-18} = 7.7 Hz, J_{19-17} = 1.5 Hz), 8.00 (dd, 1H, *H-16*, J_{16-15} = 5.8 Hz, J_{16-14} = 1.5 Hz), 7.90 (dd, 1H, *H-9*, J_{9-10} = 5.5 Hz, J_{9-11} = 1.6 Hz), 7.71 (m, 2H, *H-8 + H-1*), 7.68 (ddd, 1H, *H-10*, J_{10-11} = 7.9 Hz, J_{10-9} = 5.5 Hz, J_{10-12} = 1.1 Hz), 7.60 (dd, 1H, *H-17*, J_{17-18} = 5.8 Hz, J_{17-19} = 1.5 Hz), 7.54 (m, 2H, *H-7 + H-2*), 7.51 (ddd, 1H, *H-15*, J_{15-14} = 7.7 Hz, J_{15-16} = 5.8 Hz, J_{15-13} = 1.4 Hz), 7.34 (ddd, 1H, *H-18*, J_{18-19} = 7.7 Hz, J_{18-17} = 5.8 Hz, J_{18-20} = 1.6 Hz), 7.01 (dd, 1H, *H-22*, J_{22-23} = 7.7 Hz, J_{22-21} = 4.7 Hz), 6.63 (dd, 1H, *H-23*, J_{23-22} = 7.7 Hz, J_{23-21} = 1.6 Hz).

4.16. Iridium (III) bis(2-phenylpyridine-N,C^3) dichloro-bridged dimer ([Ir(ppy)$_2$(μ-Cl)]$_2$)

Iridium(III) chloride hydrate (694.3 mg, 1.96 mmol) was suspended in a 2-ethoxyethanol:H_2O / 3:1 mixture (31.6 mL) followed by 2-phenylpyridine (0.608 mL, 4.25 mmol). The system was kept under argon and heated to reflux overnight. The yellow solid was centrifuged, washed successively with ethanol and acetone and dissolved in dichloromethane to remove impurities. The solvents was evaporated under reduced pressure to provide a yellow solid (781.0 mg, 74 % yield). ^{1}H NMR ($CDCl_3$), δ/ppm: 9.24 (dd, 4H, *H-1*, J_{1-2} = 5.8 Hz, J_{1-3} = 1.2 Hz), 7.87 (dd, 4H, *H-4*, J_{4-3} = 8.0 Hz, J_{4-2} = 1.2 Hz), 7.73 (ddd, 4H, *H-3*, J_{3-4} = 8.0 Hz, J_{3-2} = 7.5 Hz, J_{3-1} = 1.2 Hz), 7.49 (dd, 4H, *H-5*, J_{5-6} = 8.2 Hz, J_{5-7} = 1.2 Hz), 6.75 (m, 8H, *H-2 + H-6*), 6.56 (ddd, 4H, *H-7*, J_{7-8} = 7.9 Hz, J_{7-6} = 7.2 Hz, J_{7-5} = 1.2 Hz), 5.93 (dd, 4H, *H-8*, J_{8-7} = 7.9 Hz, J_{8-6} = 0.8 Hz).

4.17. Bis (2-phenylpyridine-N,C^3) (2,2′-bipyridine-N,N') iridium(III) hexafluorophosphate [IrN$_4$C$_2$]$^+$ (5)

[Ir(ppy)$_2$(μ-Cl)]$_2$ (15.5 mg, 0.0145 mmol) was mixed with 2,2′-bipyridine (5.4 mg, 0.0347 mmol) and NH_4PF_6 (35.4 mg, 0.217 mmol) in a CH_3CN:EtOH / 3:1 mixture (2.5 mL). The mixture was kept under argon and refluxed for 24 h. The reaction mixture was cooled to room temperature and water was added. The precipitate was centrifuged, washed successively with water, ethanol and diethylether and dried under reduced pressure to afford a yellow solid (20.4 mg, 88 %). ^{1}H NMR (CD_3CN), δ/ppm: 8.53 (dd, 2H, *H-12*, J_{12-11} = 8.1 Hz, J_{12-10} = 1.3 Hz), 8.12 (ddd, 2H, *H-11*, J_{11-12} = 8.1 Hz, J_{11-10} = 7.9 Hz, J_{11-9} = 1.7 Hz), 8.06 (dd, 2H, *H-4*, J_{4-3} = 8.5 Hz, J_{4-2} = 1.6 Hz), 7.98 (dd, 2H, *H-9*, J_{9-10} = 5.5 Hz, J_{9-11} = 1.7 Hz), 7.85 (ddd, 2H, *H-3*, J_{3-4} = 8.5 Hz, J_{3-2} = 7.6 Hz, J_{3-1} = 1.6 Hz), 7.80 (dd, 2H, *H-5*, J_{5-6} = 7.8 Hz, J_{5-7} = 1.4 Hz), 7.60 (dd, 2H, *H-1*, J_{1-2} = 5.8 Hz, J_{1-3} = 1.6 Hz), 7.50 (ddd, 2H, *H-10*, J_{10-11} = 7.9 Hz, J_{10-9} = 5.5 Hz, J_{10-12} = 1.3 Hz), 7.04 (ddd, 2H, *H-6*, J_{6-5} = 7.8 Hz, J_{6-7} = 7.5 Hz, J_{6-8} = 1.3 Hz), 7.02 (ddd, 2H, *H-2*, J_{2-3} = 7.6 Hz, J_{2-1} = 5.8 Hz, J_{2-4} = 1.6 Hz), 6.92 (ddd, 2H, *H-7*, J_{7-6} = J_{7-8} = 7.5 Hz, J_{7-5} = 1.4 Hz), 6.28 (dd, 2H, *H-8*, J_{8-7} = 7.5 Hz, J_{8-6} = 1.3 Hz).

4.18. Tris (2,2′-bipyridine-N,N') iridium(III) hexafluorophosphate [IrN$_6$]$^{3+}$ (6)

2,2′-bipyridine (0.1114, 0.713 mmol) was suspended in ethylene glycol (6,5 mL) and the mixture was deoxygenated and kept under argon. [Ir(bpy)$_2$(OTf)$_2$]OTf (34.0 mg, 0.0357 mmol) was added and the suspension was heated to reflux for 5 h. The reaction mixture was cooled to room temperature. A saturated aqueous solution of KPF_6 (5 mL) was added for precipitation. The precipitate was washed with water and dried under vacuum. The remaining solid was washed with diethylether and dried (31.2 mg, 80 %). HRMS (ESI): *m/z* calculated for $[C_{30}H_{24}F_{12}^{193}IrN_6P_2 - PF_6]^+$, 951.09698 ; found: 951.09651, *m/z* calculated for $[C_{30}H_{24}F_6^{193}IrN_6P - 2\,PF_6]^{2+}$, 403.06613 ; found: 403.06593. ^{1}H NMR (CD_3CN), δ/ppm: 8.66 (dd, 6H, *H-4*, J_{4-3} = 8.3 Hz, J_{4-2} = 1.3 Hz), 8.39 (ddd, 6H, *H-3*, J_{3-4} = 8.3 Hz, J_{3-2} = 7.4 Hz, J_{3-1} = 1.4 Hz), 7.68 (m, 12H, *H-1 + H-2*).

4.19. Bis (2-phenylpyridine-N,C^3) bis (acetonitrile-N) iridium(III) hexafluorophosphate

[Ir(ppy)$_2$(μ-Cl)]$_2$ (27.9 mg, 0.0260 mmol) was suspended in CH_3CN (15.0 mL) and the mixture was kept under argon and heated to 60 °C. A solution of $AgPF_6$ (14.3 mg, 0.0567 mmol) in CH_3CN (5.0 mL) was added and the mixture was stirred at 60 °C for 2 h. The reaction mixture was cooled to room temperature and then centrifuged. The solid was washed with CH_3CN and the filtrate was evaporated under reduced pressure to afford a light-yellow solid (37.9 mg, quantitative yield). ^{1}H NMR ($CDCl_3$), δ/ppm: 8.98 (dd, 2H, *H-1*, J_{1-2} = 5.8 Hz, J_{1-3} = 1.2 Hz), 7.92 (m, 4H, *H-3 + H-4*), 7.54 (dd, 2H, *H-5*, J_{5-6} = 7.7 Hz, J_{5-7} = 1.3 Hz), 7.40 (dd, 2H, *H-2*, J_{2-1} = 5.8 Hz, J_{2-3} = 3.2 Hz), 6.86 (ddd, 2H, *H-6*, J_{6-5} = 7.7 Hz, J_{6-7} = 7.5 Hz, J_{6-8} = 1.2 Hz), 6.71 (ddd, 2H, *H-7*, J_{7-6} = J_{7-8} = 7.5 Hz, J_{7-5} = 1.3 Hz), 6.03 (dd, 2H, *H-8*, J_{8-7} = 7.5 Hz, J_{8-6} = 1.2 Hz), 2.26 (s, 6H, *H-Me*).

4.20. Tris (2-phenylpyridine-N,C^3) iridium(III) [IrN$_3$C$_3$] (7)

[Ir(ppy)$_2$(CH_3CN)$_2$]PF_6 (37.9 mg, 0.0521 mmol) was suspended in a solution of 2-phenylpyridine (8.9 μL, 0.0625 mmol) in *o*-dichlorobenzene (5.0 mL). The mixture was then kept under argon and heated to 100 °C for 5 days. The solution was cooled to room temperature and directly purified by column chromatography on silica gel using hexane as eluent to remove the solvent and then dichloromethane. Evaporation of the solvents afforded a bright yellow solid (16.1 mg, 47 %). ^{1}H NMR (CD_3CN), δ/ppm: 8.01 (dd, 3H, *H-4*, J_{4-3} = 8.3 Hz, J_{4-2} = 1.1 Hz), 7.72

(m, 6H, *H-3* + *H-5*), 7.60 (dd, 3H, *H-1*, $J_{1-2} = 5.6$ Hz, $J_{1-3} = 1.7$ Hz), 7.00 (ddd, 3H, *H-2*, $J_{2-3} = 7.4$ Hz, $J_{2-1} = 5.6$ Hz, $J_{2-4} = 1.1$ Hz), 6.86 (ddd, 3H, *H-6*, $J_{6-7} = 7.7$ Hz, $J_{6-5} = 7.1$ Hz, $J_{6-8} = 1.4$ Hz), 6.74 (ddd, 3H, *H-7*, $J_{7-6} = 7.7$ Hz, $J_{7-8} = 7.5$ Hz, $J_{7-5} = 1.4$ Hz), 6.68 (ddd, 3H, *H-8*, $J_{8-7} = 7.5$ Hz, $J_{8-6} = 1.4$ Hz).

CRediT authorship contribution statement

Cédric Lentz: Conceptualization, Methodology, Formal analysis, Validation, Investigation, Writing - original draft. **Lionel Marcélis:** Investigation, Writing - original draft. **Ludovic Troian-Gautier:** Formal analysis, Validation, Investigation, Writing - original draft, Writing - review & editing. **Koen Robeyns:** Investigation. **Emilie Cauët:** Formal analysis, Investigation, Methodology. **Benjamin Elias:** Conceptualization, Supervision, Funding acquisition, Investigation, Project administration, Writing - review & editing.

Declaration of Competing Interest

The authors declare that they have no known competing financial interests or personal relationships that could have appeared to influence the work reported in this paper.

Acknowledgements

The authors gratefully acknowledge the *Région Wallonne*, the *Université catholique de Louvain* and the *Prix Pierre et Colette Bauchau* for financial support. L. T.-G. is a postdoctoral researcher of the Fonds de la Recherche Scientifique - FNRS. The authors are also grateful to Prof. F. Loiseau, Prof. M. Luhmer and Dr. S. Wehlin for their scientific contributions. Computational resources have been provided by the Shared ICT Services Centre, Université Libre de Bruxelles.

Appendix A. Supplementary data

Supplementary material related to this article can be found, in the online version, at doi:https://doi.org/10.1016/j.jphotochem.2020.112957.

References

[1] D. Di Censo, S. Fantacci, F. De Angelis, C. Klein, N. Evans, K. Kalyanasundaram, H. J. Bolink, M. Grätzel, M.K. Nazeeruddin, Synthesis, Characterization, and DFT/TD-DFT Calculations of Highly Phosphorescent Blue Light-Emitting Anionic Iridium Complexes, Inorg. Chem. 47 (2008) 980–989.

[2] K.A. McGee, K.R. Mann, Selective low-temperature syntheses of facial and meridional tris-cyclometalated iridium(III) complexes, Inorg. Chem. 46 (2007) 7800–7809.

[3] M.K. Nazeeruddin, R.T. Wegh, Z. Zhou, C. Klein, Q. Wang, F. De Angelis, S. Fantacci, M. Grätzel, Efficient green-blue-Light-Emitting cationic iridium complex for light-emitting electrochemical cells, Inorg. Chem. 45 (2006) 9245–9250.

[4] E. Baranoff, B.F.E. Curchod, J. Frey, R. Scopelliti, F. Kessler, I. Tavernelli, U. Rothlisberger, M. Grätzel, M.K. Nazeeruddin, Acid-Induced Degradation of Phosphorescent Dopants for OLEDs and Its Application to the Synthesis of Tris-heteroleptic Iridium(III) Bis-cyclometalated Complexes, Inorg. Chem. 51 (2012) 215–224.

[5] S. Jung, Y. Kang, H.-S. Kim, Y.-H. Kim, C.-L. Lee, J.-J. Kim, S.-K. Lee, S.-K. Kwon, Effect of substitution of methyl groups on the luminescence performance of IrIII complexes: preparation, structures, electrochemistry, photophysical properties and their applications in organic light-emitting diodes (OLEDs), Eur. J. Inorg. Chem. 2004 (2004) 3415–3423.

[6] M. Mauro, K.C. Schuermann, R. Prétôt, A. Hafner, P. Mercandelli, A. Sironi, L. De Cola, Complex iridium(III) salts: luminescent porous crystalline materials, Angew. Chem. Int. Ed. 49 (2010) 1222–1226.

[7] X. Ren, M.E. Kondakova, D.J. Giesen, M. Rajeswaran, M. Madaras, W.C. Lenhart, Coumarin-Based, Electron-Trapping Iridium Complexes as Highly Efficient and Stable Phosphorescent Emitters for Organic Light-Emitting Diodes, Inorg. Chem. 49 (2010) 1301–1303.

[8] K.-H. Leung, H.-Z. He, V. Ma, H.-J. P.-Y.; Zhong, D. Chan, J. S.-H.; Zhou, J.-L. Mergny, C.-H. Leung, D.-L. Ma, Detection of base excision repair enzyme activity using a luminescent G-quadruplex selective switch-on probe, Chem. Commun. (Camb.) 49 (2013) 5630–5632.

[9] P. Steunenberg, A. Ruggi, N.S. van den Berg, T. Buckle, J. Kuil, F.W.B. van Leeuwen, A.H. Velders, Phosphorescence imaging of living cells with amino acid-functionalized tris(2-phenylpyridine)iridium(III) complexes, Inorg. Chem. 51 (2012) 2105–2114.

[10] Z. Wu, J. Mu, Q. Wang, X. Chen, L. Jensen, C. Yi, M.-J. Li, Hydroxyl and amino functionalized cyclometalated Ir(III) complexes: synthesis, characterization and cytotoxicity studies, J. Organomet. Chem. 791 (2015) 175–182.

[11] B.F. DiSalle, S. Bernhard, Orchestrated photocatalytic water reduction using surface-adsorbing iridium photosensitizers, J. Am. Chem. Soc. 133 (2011) 11819–11821.

[12] A. Fihri, V. Artero, A. Pereira, M. Fontecave, Efficient H2-producing photocatalytic systems based on cyclometalated iridium- and tricarbonylrhenium-diimine photosensitizers and cobaloxime catalysts, Dalton Trans. (2008) 5567–5569.

[13] R. Bevernaegie, S.A.M. Wehlin, E.J. Piechota, M. Abraham, C. Philouze, G. J. Meyer, B. Elias, L. Troian-Gautier, Improved visible light absorption of potent iridium(III) photo-oxidants for excited-state Electron transfer chemistry, J. Am. Chem. Soc. 142 (2020) 2732–2737.

[14] P. Govindaswamy, J. Canivet, B. Therrien, G. Süss-Fink, P. Štěpnička, J. Ludvík, Mono and dinuclear rhodium, iridium and ruthenium complexes containing chelating 2,2′-bipyrimidine ligands: synthesis, molecular structure, electrochemistry and catalytic properties, J. Organomet. Chem. 692 (2007) 3664–3675.

[15] N. Hoffmann, Combining photoredox and metal catalysis, ChemCatChem 7 (2015) 393–394.

[16] J. Xuan, T.-T. Zeng, Z.-J. Feng, Q.-H. Deng, J.-R. Chen, L.-Q. Lu, W.-J. Xiao, H. Alper, Redox-neutral α-Allylation of amines by combining palladium catalysis and visible-light photoredox catalysis, Angew. Chem. Int. Ed. 54 (2015) 1625–1628.

[17] J. Zoller, D.C. Fabry, M.A. Ronge, M. Rueping, Synthesis of Indoles Using Visible Light: Photoredox Catalysis for Palladium-Catalyzed C□H Activation, Angew. Chem. Int. Ed. 53 (2014) 13264–13268.

[18] C.M. Morton, Q. Zhu, H. Ripberger, L. Troian-Gautier, Z.S.D. Toa, R.R. Knowles, E. J. Alexanian, C–H alkylation via multisite-proton-Coupled Electron transfer of an aliphatic C–H bond, J. Am. Chem. Soc. 141 (2019) 13253–13260.

[19] B. Xu, L. Troian-Gautier, R. Dykstra, R.T. Martin, O. Gutierrez, U.K. Tambar, Photocatalyzed diastereoselective isomerization of cinnamyl chlorides to Cyclopropanes, J. Am. Chem. Soc. 142 (2020) 6206–6215.

[20] J. Li, P.I. Djurovich, B.D. Alleyne, M. Yousufuddin, N.N. Ho, J.C. Thomas, J. C. Peters, R. Bau, M.E. Thompson, Synthetic control of excited-state properties in cyclometalated Ir(III) complexes using ancillary ligands, Inorg. Chem. 44 (2005) 1713–1727.

[21] I.M. Dixon, J.-P. Collin, J.-P. Sauvage, L. Flamigni, S. Encinas, F. Barigelletti, A family of luminescent coordination compounds: iridium(III) polyimine complexes, Chem. Soc. Rev. 29 (2000) 385–391.

[22] L. Flamigni, A. Barbieri, C. Sabatini, B. Ventura, F. Barigelletti, Photochemistry and photophysics of coordination compounds: iridium, in: V. Balzani, S. Campagna (Eds.), Photochemistry and Photophysics of Coordination Compounds II, Springer Berlin Heidelberg, Berlin, Heidelberg, 2007, pp. 143–203.

[23] S. Aoki, Y. Matsuo, S. Ogura, H. Ohwada, Y. Hisamatsu, S. Moromizato, M. Shiro, M. Kitamura, Regioselective aromatic substitution reactions of cyclometalated Ir (III) complexes: synthesis and photochemical properties of substituted Ir(III) complexes that exhibit blue, Green, and red color luminescence emission, Inorg. Chem. 50 (2011) 806–818.

[24] E.C. Constable, M. Neuburger, P. Rösel, G.E. Schneider, J.A. Zampese, C. E. Housecroft, F. Monti, N. Armaroli, R.D. Costa, E. Ortí, Ligand-based charge-transfer luminescence in ionic cyclometalated iridium(III) complexes bearing a pyrene-functionalized bipyridine ligand: a joint theoretical and experimental study, Inorg. Chem. 52 (2013) 885–897.

[25] K. Dedeian, J. Shi, N. Shepherd, E. Forsythe, D.C. Morton, Photophysical and electrochemical properties of heteroleptic tris-cyclometalated iridium(III) complexes, Inorg. Chem. 44 (2005) 4445–4447.

[26] J.I. Goldsmith, W.R. Hudson, M.S. Lowry, T.H. Anderson, S. Bernhard, Discovery and high-throughput screening of heteroleptic iridium complexes for photoinduced hydrogen production, J. Am. Chem. Soc. 127 (2005) 7502–7510.

[27] J.I. Kim, I.-S. Shin, H. Kim, J.-K. Lee, Efficient electrogenerated chemiluminescence from cyclometalated iridium(III) complexes, J. Am. Chem. Soc. 127 (2005) 1614–1615.

[28] M. Rueping, C. Vila, Visible light photoredox-catalyzed multicomponent reactions, Org. Lett. 15 (2013) 2092–2095.

[29] T. Sajoto, P.I. Djurovich, A.B. Tamayo, J. Oxgaard, W.A. Goddard, M.E. Thompson, Temperature dependence of blue phosphorescent cyclometalated Ir(III) complexes, J. Am. Chem. Soc. 131 (2009) 9813–9822.

[30] F. Shao, B. Elias, W. Lu, J.K. Barton, Synthesis and characterization of iridium(III) cyclometalated complexes with oligonucleotides: insights into redox reactions with DNA, Inorg. Chem. 46 (2007) 10187–10199.

[31] V.L. Whittle, J.A.G. Williams, A new class of iridium complexes suitable for stepwise incorporation into linear assemblies: synthesis, electrochemistry, and luminescence, Inorg. Chem. 47 (2008) 6596–6607.

[32] C.-H. Yang, K.-H. Fang, C.-H. Chen, I.W. Sun, High efficiency mer-iridium complexes for organic light-emitting diodes, Chem. Commun. (2004) 2232–2233.

[33] T. Yu, Y. Zeng, J. Chen, Y.-Y. Li, G. Yang, Y. Li, Exceptional dendrimer-based mimics of Diiron Hydrogenase for the photochemical production of hydrogen, Angew. Chem. Int. Ed. 52 (2013) 5631–5635.

[34] K.A. King, P.J. Spellane, R.J. Watts, Excited-state properties of a triply ortho-metalated iridium(III) complex, J. Am. Chem. Soc. 107 (1985) 1431–1432.

[35] W. Holzer, A. Penzkofer, T. Tsuboi, Absorption and emission spectroscopic characterization of Ir(ppy)3, Chem. Phys. 308 (2005) 93–102.
[36] S.-H. Wu, J.-W. Ling, S.-H. Lai, M.-J. Huang, C.H. Cheng, I.C. Chen, Dynamics of the excited states of [Ir(ppy)2bpy]+ with triple phosphorescence, J. Phys. Chem. A 114 (2010) 10339–10344.
[37] K. Ichimura, T. Kobayashi, K.A. King, R.J. Watts, Excited-state absorption spectroscopy of ortho-metalated iridium(III) complexes, J. Phys. Chem. 91 (1987) 6104–6106.
[38] A.A. Abdel-Shafi, J.L. Bourdelande, S.S. Ali, Photosensitized generation of singlet oxygen from rhenium(i) and iridium(iii) complexes, Dalton Trans. (2007) 2510–2516.
[39] E.C. Constable, T.A. Leese, Metal exchange in organomercury complexes; a facile route to cyclometallated transition metal complexes, J. Organomet. Chem. 335 (1987) 293–299.
[40] M.F. Finlayson, P.C. Ford, R.J. Watts, Excited states and transients formed in laser flash photolysis of iridium(III) complexes of 2,2'-bipyridine, J. Phys. Chem. 90 (1986) 3916–3922.
[41] K.A. King, R.J. Watts, Dual emission from an ortho-metalated iridium(III) complex, J. Am. Chem. Soc. 109 (1987) 1589–1590.
[42] B. Minaev, H. Ågren, F.D. Angelis, Theoretical design of phosphorescence parameters for organic electro-luminescence devices based on iridium complexes, Chem. Phys. 358 (2009) 245–257.
[43] S. Soman, H.M. Younis, W.R. Browne, J.G. Vos, M.T. Pryce, Synthesis and isotope effects on the excited state properties of N^N bound [Ir(polypyridyl)2Cl2]PF6 complexes, Eur. J. Inorg. Chem. 2017 (2017) 5598–5603.
[44] R.J. Watts, J.S. Harrington, J. Van Houten, A stable monodentate 2,2'-bipyridine complex of iridium(III): a model for reactive intermediates in ligand displacement reactions of tris-2,2'-bipyridine metal complexes, J. Am. Chem. Soc. 99 (1977) 2179–2187.
[45] A. Slama-Schwok, S. Gershuni, J. Rabani, H. Cohen, D. Meyerstein, An iridium-bipyridine complex as a photosensitizer for the bromide oxidation to bromine by oxygen, J. Phys. Chem. 89 (1985) 2460–2464.
[46] A. Slama-Schwok, J. Rabani, Photochemical oxidation of [Ir((C3,N'-Hbpy)(bpy)2)]3+ by redox quenching, J. Phys. Chem. 90 (1986) 1176–1179.
[47] D. Behar, P. Neta, J. Silverman, J. Rabani, The reaction of [Ir(C3,N′-bpy) (bpy)2]2+ with OH radicals and radiation induced covalent binding of the complex to several polymers in aqueous solutions, Radiat. Phys. Chem. Int. J. Radiat. Appl. Instrum., Part C 29 (1987) 253–260.
[48] R.M. O'Donnell, R.N. Sampaio, G. Li, P.G. Johansson, C.L. Ward, G.J. Meyer, Photoacidic and photobasic behavior of transition metal compounds with carboxylic acid group(s), J. Am. Chem. Soc. 138 (2016) 3891–3903.
[49] E.N. Dixon, M.Z. Snow, J.L. Bon, A.M. Whitehurst, B.A. DeGraff, C. Trindle, J. N. Demas, Environmental sensitivity of Ru(II) complexes: the role of the accessory ligands, Inorg. Chem. 51 (2012) 3355–3365.
[50] C. Hicks, G. Ye, C. Levi, M. Gonzales, I. Rutenburg, J. Fan, R. Helmy, A. Kassis, H. D. Gafney, Excited-state acid–base chemistry of coordination complexes, Coord. Chem. Rev. 211 (2001) 207–222.
[51] B. Higgins, B.A. DeGraff, J.N. Demas, Luminescent transition metal complexes as sensors: structural effects on pH response, Inorg. Chem. 44 (2005) 6662–6669.
[52] P.A. Lay, W.H.F. Sasse, Proton transfer in the excited state of carboxylic acid derivatives of tris(2,2'-bipyridine-N,N')ruthenium(II), Inorg. Chem. 23 (1984) 4123–4125.
[53] M.K. Nazeeruddin, K. Kalyanasundaram, Acid-base behavior in the ground and excited states of ruthenium(II) complexes containing tetraimines or dicarboxybipyridines as protonatable ligands, Inorg. Chem. 28 (1989) 4251–4259.
[54] S.H. Peterson, J.N. Demas, Excited state acid-base reactions of transition metal complexes: dicyanobis(2,2'-bipyridine) ruthenium(III) in aqueous acid, J. Am. Chem. Soc. 98 (1976) 7880–7881.
[55] H. Shizuka, Excited-state proton-transfer reactions and proton-induced quenching of aromatic compounds, Acc. Chem. Res. 18 (1985) 141–147.
[56] L.M. Tolbert, K.M. Solntsev, Excited-state proton transfer: from constrained systems to "Super" photoacids to superfast proton transfer, Acc. Chem. Res. 35 (2002) 19–27.
[57] J.G. Vos, Excited-state acid-base properties of inorganic compounds, Polyhedron 11 (1992) 2285–2299.
[58] A. Jacques, O. Schott, K. Robeyns, G.S. Hanan, B. Elias, Hydrogen photoevolution from a green-absorbing iridium(III)–Cobalt-(III) dyad, Eur. J. Inorg. Chem. 2016 (2016) 1779–1783.
[59] C. Lentz, O. Schott, T. Auvray, G.S. Hanan, B. Elias, Design and photophysical studies of iridium(iii)–cobalt(iii) dyads and their application for dihydrogen photo-evolution, Dalton Trans. 48 (2019) 15567–15576.
[60] C. Lentz, O. Schott, T. Auvray, G. Hanan, B. Elias, Photocatalytic hydrogen production using a red-absorbing Ir(III)–Co(III) dyad, Inorg. Chem. 56 (2017) 10875–10881.
[61] F.O. Garces, R.J. Watts, A new ortho-metalated dichloro-bridged complex of iridium(III) with 2,2'-bipyridine: [{Ir(bpy-C3,N')(bpy-N,N')Cl}2][Cl]2, Inorg. Chem. 29 (1990) 582–584.
[62] C.R. Groom, I.J. Bruno, M.P. Lightfoot, S.C. Ward, The cambridge structural database, Acta Crystallogr. B 72 (2016) 171–179.
[63] N. Matsuo, Benzo[h]quinolin-10-yl-N iridium(III) complexes, B. Chem. Soc. Jpn. 47 (1974) 767–768.
[64] G. Berger, L. Fusaro, M. Luhmer, J. Czapla-Masztafiak, E. Lipiec, J. Szlachetko, Y. Kayser, D.L.A. Fernandes, J. Sá, F. Dufrasne, S. Bombard, Insights into the structure–activity relationships of chiral 1,2-diaminophenylalkane platinum(II) anticancer derivatives, J. Biol. Inorg. Chem. 20 (2015) 841–853.
[65] A. Krężel, W. Bal, A formula for correlating pKa values determined in D2O and H2O, J. Inorg. Biochem. 98 (2004) 161–166.
[66] Y. Naokazu, M. Yoshitaka, M.-I. Takeko, Rapid synthesis of new emitting Ir(III) polypyridine complexes, Chem. Lett. 29 (2000) 1206–1207.
[67] L. Troian-Gautier, C. Moucheron, RutheniumII complexes bearing fused polycyclic ligands: from fundamental aspects to potential applications, Molecules 19 (2014) 5028–5087.
[68] K. Hasan, A.K. Bansal, I.D.W. Samuel, C. Roldán-Carmona, H.J. Bolink, E. Zysman-Colman, Tuning the emission of cationic iridium (III) complexes towards the red through methoxy substitution of the cyclometalating ligand, Sci. Rep. 5 (2015) 12325.
[69] R. Bevernaegie, L. Marcélis, B. Laramée-Milette, J. De Winter, K. Robeyns, P. Gerbaux, G.S. Hanan, B. Elias, Trifluoromethyl-substituted iridium(III) complexes: from photophysics to photooxidation of a biological target, Inorg. Chem. 57 (2018) 1356–1367.
[70] L. Wang, S. Monro, P. Cui, H. Yin, B. Liu, C.G. Cameron, W. Xu, M. Hetu, A. Fuller, S. Kilina, S.A. McFarland, W. Sun, Heteroleptic Ir(III)N6 complexes with long-lived triplet excited states and in vitro photobiological activities, ACS Appl. Mater. Interfaces 11 (2019) 3629–3644.
[71] S. Takayasu, T. Suzuki, K. Shinozaki, Intermolecular interactions and aggregation of fac-tris(2-phenylpyridinato-C2,N)iridium(III) in Nonpolar Solvents, J. Phys. Chem. B 117 (2013) 9449–9456.
[72] J.C. Deaton, C.M. Taliaferro, C.L. Pitman, R. Czerwieniec, E. Jakubikova, A.J. M. Miller, F.N. Castellano, Excited-state switching between ligand-centered and charge transfer modulated by metal–Carbon bonds in cyclopentadienyl iridium complexes, Inorg. Chem. 57 (2018) 15445–15461.
[73] R.D. Egeland, F. Marken, E.M. Southern, An electrochemical redox couple activitated by microelectrodes for confined chemical patterning of surfaces, Anal. Chem. 74 (2002) 1590–1596.
[74] S.L. Murov, I. Carmichael, G.L. Hug, Handbook of Photochemistry, 2nd edition, Marcel Dekker, Inc., New York, 1993.
[75] Rigaku Oxford Diffraction, C. P. S. s., Version 1.171.34.40, 2010 or Version 1.171.36.21, Rigaku Corporation, Oxford, UK, 2012.
[76] G. Sheldrick, A short history of SHELX, Acta Crystallogr. A 64 (2008) 112–122.
[77] A. Spek, Structure validation in chemical crystallography, Acta Crystallogr. D 65 (2009) 148–155.
[78] M.J. Frisch, G.W. Trucks, H.B. Schlegel, G.E. Scuseria, M.A. Robb, J.R. Cheeseman, et al., Gaussian 09., Revision D.01.01,. Gaussian, Inc., Wallingford CT, 2016.
[79] G. Scalmani, M.J. Frisch, Continuous surface charge polarizable continuum models of solvation. I. General formalism, J. Chem. Phys. 132 (2010), 114110.
[80] A.D. Becke, Density-functional exchange-energy approximation with correct asymptotic behavior, Phys. Rev. A (Coll Park) 38 (1988) 3098–3100.
[81] C. Lee, W. Yang, R.G. Parr, Development of the Colle-Salvetti correlation-energy formula into a functional of the electron density, Phys. Rev. B 37 (1988) 785–789.
[82] B. Miehlich, A. Savin, H. Stoll, H. Preuss, Results obtained with the correlation energy density functionals of becke and Lee, Yang and Parr, Chem. Phys. Lett. 157 (1989) 200–206.
[83] T. Clark, J. Chandrasekhar, G.W. Spitznagel, P.V.R. Schleyer, Efficient diffuse function-augmented basis sets for anion calculations. III. The 3-21+G basis set for first-row elements, Li–F, J. Comput. Chem. 4 (1983) 294–301.
[84] P.C. Hariharan, J.A. Pople, The influence of polarization functions on molecular orbital hydrogenation energies, Theor. Chim. Acta 28 (1973) 213–222.
[85] W.J. Hehre, R. Ditchfield, J.A. Pople, Self—consistent molecular orbital methods. XII. Further extensions of gaussian—type basis sets for use in molecular orbital studies of organic molecules, J. Chem. Phys. 56 (1972) 2257–2261.
[86] W.J. Stevens, M. Krauss, H. Basch, P.G. Jasien, Relativistic compact effective potentials and efficient, shared-exponent basis sets for the third-, fourth-, and fifth-row atoms, Can. J. Chem. 70 (1992) 612–630.